CENTRAL RESEARCH LIBRARY

OAK RIDGE NATIONAL LABORATORY
OPERATED BY
UNION CARBIDE CORPORATION
NUCLEAR DIVISION

POST OFFICE BOX X
OAK RIDGE, TENNESSEE 37830

ORNL-MIT-192

DATE: May 22, 1974 COPY NO. 31

SUBJECT: Comparison of Flat Plate and Cylindrical Parabolic Focusing Solar Energy Collectors for Oak Ridge

AUTHOR: E.J. Kronenberger, J.S. Newman, C.V. Demetriou, and R.D. Orlandi*

Consultant: A.P. Fraas

DO NOT TRANSFER TO ANOTHER PERSON
If you wish someone else to see this document, send in name with document and the library will arrange a loan.
UCN-7969 (3 3-67)

ABSTRACT [redacted]

Experimental and theoretical comparisons were made of the performance of cylindrical parabolic and flat plate solar energy collectors operating under Oak Ridge weather conditions. The flat plate collector was observed to consistently out-perform the parabolic collector under the design and operating (135-185°F) conditions used (parabolic cylindrical collector - one glass cover plate, refocused hourly, receiver absorptivity of 0.87; flat plate collector - two glass cover plates, oriented at latitude minus declination, absorptivity 0.98). Other factors contributed to the difference including poorer insulation (1.25 in. fiberglass) for the focusing collector (versus 5 in. fiberglass for the flat plate) and a poor fin efficiency for the receiver tube of the focusing collector. Observed efficiencies were as high as 47% for the cylindrical parabolic collector operating with one glass plate at 185°F and as high as 62% for the flat plate collector operating with two glass plates at 165°F. Performance models were developed for both collectors and the model used for the flat plate collector was extended to predict month-to-month operation under Oak Ridge weather conditions (based on the average of 16 years of weather data). A temperature distribution model was developed for optimization of the finned tube receiver used in the cylindrical parabolic collector. Further experimentation should be conducted at higher temperatures (~250°F) with selective receiver coatings ($\alpha/\varepsilon >> 1$) and also runs under conditions of broken cloud cover are suggested. In addition, the performance models should be extended and the finned tube design optimization continued.

*Revised in part by J.W. Tester and R.M. Mayer

Oak Ridge Station
School of Chemical Engineering Practice
Massachusetts Institute of Technology

[redacted]

OAK RIDGE NATIONAL LABORATORY
CENTRAL RESEARCH LIBRARY
DOCUMENT COLLECTION
LIBRARY LOAN COPY

Contents

Page

1. Summary 4
2. Introduction 6
   2.1 Justification 6
   2.2 Background 6
   2.3 Objectives and Method of Attack 7
3. Seasonal and Diurnal Movement of the Sun 7
4. Theoretical Characteristics of Finned Tube Performance 14
5. Apparatus and Procedure 15
   5.1 Apparatus 15
   5.2 Procedure 19
6. Results and Discussion 21
   6.1 Experimental Results 21
   6.2 Comparison Between Observed and Theoretical Useful Heat Gained by Working Fluid for the Flat Plate and Parabolic Focusing Solar Energy Collectors 24
   6.3 Monthly Efficiencies for Oak Ridge Weather Conditions 26
7. Conclusions 32
8. Recommendations 33
9. Acknowledgements 34
10. Appendix 35
   10.1 Performance Equations 35
   10.2 Sample Calculations 41
   10.3 Theoretical Development of Efficiencies Based on Monthly Averages 47
   10.4 Development of Temperature Distribution Along Finned Tube . 58
   10.5 Location of Original Data 67
   10.6 Dimensions and Properties of Materials 67
   10.7 Nomenclature 73
   10.8 Temperature Measurements 73
   10.9 References 73

1. SUMMARY

Theoretical and experimental comparisons were made between the performance of a cylindrical parabolic and a flat plate solar energy collector operating simultaneously under Oak Ridge weather conditions. Data of this type are required to determine the optimal collector design for use under any defined weather conditions. Performance variables of interest were operating temperatures and corresponding efficiencies. One design variable was examined (the number of glass cover plates), and two operating variables were investigated (unit orientation and operating temperature). Efficiencies were defined as the ratio of the amount of useful heat transferred to the working fluid (water) to the amount of insolation incident upon the active area of each unit (aperture area of cylindrical parabolic collector and total area of flat plate collector).

Experimental comparisons were accomplished by use of two collectors housed in fiberglass insulated plywood boxes with provision for one or two glass cover plates. The cylindrical parabolic collector consisted of an Alzak aluminum reflector (reflectivity ~87%) 90-in. long x 18.5-in. wide (2.29-m long x 0.47-m wide) and a 0.5-in.-diam galvanized steel pipe receiver with two vertically positioned brass fins (90-in. long x 0.67-in. wide x 0.01-in. thick). The flat plate collector consisted of a roll-bonded sheet [17 in. x 50 in. (0.557 m x 1.64 m)] of aluminum with six parallel channels [~15.26 in.^{3} (250 cm^3) total volumetric capacity]. The finned receiver was coated with a black paint of ~0.87 absorptivity and emissivity while the entire exposed surface of the flat plate collector was coated with a carbon based black paint of 0.98 absorptivity and emissivity. The aperture area of the focusing device was 11.56 ft^2 (1.07 m^2) compared to 5.9 ft^2 (0.548 m^2) for the flat plate. Both collectors were positioned horizontally in an east-west orientation at a tilt angle equivalent to the latitude minus the solar declination δ for that day. Temperatures, flow rates, diffuse and total incident radiation (measured with Eppley pyrheliometers), and wind speeds were recorded continuously during each experiment. Outlet temperatures from each unit were held constant during each experiment by control of water flow rates through the receivers. Operating outlet temperatures of 135, 165, and 185°F were investigated.

Theoretical comparisons of collector performance were based upon models developed in the literature and by a previous MIT study (13) modified to represent the operation of the units used in our experimental studies. The performance model used for the flat plate collector was extended to describe the month-to-month operation using Oak Ridge weather data collected over the past sixteen years.

Experimental results indicated that one and two layers of 0.125-in.-thick glass plates should be used for operation of the cylindrical parabolic and flat plate collectors, respectively, at the operating temperatures studied. The performance of the flat plate collector showed that for Oak Ridge weather conditions an orientation of 36° from the vertical (equal to the latitude at Oak Ridge) was near optimum. A temperature distribution model was developed to describe the operation of the finned tube used as a

receiver in the cylindrical parabolic collector under various pointing angle errors, but no optimum orientation was calculated.

Experimental efficiencies varied from 17 to 47% for the cylindrical parabolic collector and from 19 to 62% for the flat plate collector. Reasonable agreement was obtained between experimental and calculated heat losses for both units indicating that performance could be estimated for average sky conditions, ambient temperatures, and wind velocities typical for yearly operation in Oak Ridge. An efficiency of 47% was achieved with the parabolic collector operating with two layers of glass cover plates at 186°F while being oriented by hourly refocusing. An efficiency of 62% was obtained with the flat plate collector operating at 163°F with two layers of glass cover plates while oriented at 18° from the vertical (latitude minus the declination). In the relatively low temperature range studied with the collector designs and for the orientations used, the flat plate collector consistently gave a higher collector efficiency than the cylindrical parabolic collector while operating. Three major causes were cited to explain the differences in performance: (1) reflectance losses at the aluminum surface (∿13%), (2) ratio of diffuse to total radiation (direct + diffuse) (up to 40%), and (3) fin efficiencies << 100% for finned receiver.

The roll-bonded aluminum flat plate collector tested is commercially available at a cost of $1.75/ft^2 and the cover glass required costs about $1.00/ft^2. The Alzak aluminum sheet for the parabolic mirror employed costs about $1.55/ft^2, the glass cover plate about $0.50/ft^2, and the finned tubing about $0.65/ft. The actual installation cost is difficult to estimate but would be higher for the parabolic mirror.

It is recommended that:

1. Further experimental investigations should be carried out at higher temperatures (∿250°F) while using a selective coating on the receiver of a second flat plate collector operating in conjunction with the collectors used in this study.

2. The cylindrical parabolic collector performance model should be improved to allow extension of month-to-month operation.

3. The optimization of the finned tube receiver used as the cylindrical parabolic receiver should be completed.

4. The experimental apparatus should be modified by the addition of thermostats and recording flowmeters to allow investigation of collector performance under conditions of broken cloud cover.

5. Alternate finned tube receiver designs should be investigated for the parabolic focusing collector to improve the collection efficiency at the absorbing surface.

6. The overall system cost as a function of collection temperature should be estimated for both types of collector. The estimates should include the costs of both heat storage and an absorption air conditioning system.

2. INTRODUCTION

2.1 Justification

As fossil fuels have become more expensive and more difficult to obtain, interest in the utilization of solar energy for space heating and cooling has increased. While solar energy provides heat without fuel costs, the capital costs associated with collectors, heat storage systems, and auxiliary heaters have previously caused this resource to be economically unattractive. With the prospect of steadily increasing fuel prices, a time can be envisioned when relative costs (fuel vs capital) will reverse, allowing the utilization of solar power by the individual home owner. There is interest, therefore, in the determination of an economically attractive collector design, particularly one suitable for a variety of different geographic locations.

2.2 Background

In a study at ORNL by Fraas, Samuels, and Wilson (7), a solar heating (hot water) and air conditoning (LiBr absorption) system was designed and evaluated economically for use in the Oak Ridge area. This particular system was designed to use cylindrical parabolic collectors that would be capable of supplying heat at ∿250°F to a pressurized water storage system.

A competing design - a flat plate collector - operates efficiently at somewhat lower temperatures (maximum of ∿200°F) and can utilize both the diffuse and direct components of solar radiation, whereas the parabolic collector utilizes only direct insolation. A flat plate collector, therefore, should perform more efficiently under hazy or cloudy conditions, which are frequently typical for the Oak Ridge area.

Previous work by Hottel and associates at MIT (9, 10) has delineated the performance of flat plate solar collectors as a function of weather (cloud cover), design parameters (number of glass cover plates, receiver design), and operating conditions (outlet temperature, orientation). Work by Löf and his co-workers (11, 12) has similarly characterized the operation of cylindrical parabolic collectors. A previous MIT Practice School group (13) investigated the operation of a specific parabolic collector (also used in this study) and was able to characterize satisfactorily the heat losses and efficiency data for a range of operating temperatures (<230°F). To date, however, little has been done to compare the operation of the two units under the same sky conditions. Such a comparison would be of particular interest for Oak Ridge which receives relatively large amounts of direct insolation during the winter and relatively small amounts during the summer (due mainly to atmospheric haze and turbidity).

2.3 Objectives and Method of Attack

The performance of a cylindrical parabolic and flat plate collector will be compared by operating them simultaneously under varied Oak Ridge weather conditions with selected design and operating conditions (number of glass cover plates, orientation, etc.). Based on our experimental findings, existing performance models will also be extended to allow prediction of collector operation for each month of the year using weather and solar radiation data collected over the past 16 years as a basis. The optimization of the finned tube receiver which was initiated by the previous MIT study (13) will be continued. Design and operating parameters were examined and fixed successively in order to approach optimal performance conditions for each unit.

3. SEASONAL AND DIURNAL MOVEMENT OF THE SUN

To take full advantage of incident solar radiation, proper alignment of the collector is critical. Knowledge of the sun's seasonal and diurnal movement relative to an observer on earth must be understood. Since focusing is required for the parabolic collector, proper alignment is critical. Even for a fixed flat plate collector optimal alignment can improve performance significantly. All required information can be determined with some basic knowledge of astronomical coordinate systems. The two coordinate systems of interest are the horizon and the equator systems (1).

Figure 1 illustrates the horizon system of coordinates. An observer located on earth (at origin O) views any celestial object as being on a dome, whose dimensions are so large that the size of the earth is negligible in comparison. This dome is part of the celestial sphere which surrounds the earth. The intersection of the celestial sphere by a plumb line extended upward from the observer's position occurs at the zenith (Z). A plane perpendicular to the ZO line and passing through the observer's position intersects the celestial sphere at the horizon circle NESW. Extension of the earth's axis of rotation into space (line PO) intersects the celestial sphere at point P, the north celestial pole (Polaris). The great circle NPZS is the observer's meridian.

The position of the sun (R) may be located at any time on the coordinate system. A line drawn perpendicular to the horizon circle passing through the sun and zenith constitutes a vertical circle. The altitude (h) is that angular distance measured from the foot of the vertical circle to the sun along the vertical circle. θ_Z is the zenith angle and is equal to 90° - h. The azimuth (A") locates the foot of the vertical circle by measurement of the angle from the north point of the horizontal circle toward the east along the horizon circle to the foot of the vertical circle (1).

Using this system for coordinates, the azimuth and altitude of the sun are purely local. Should the observer change his position, the sun's location will vary accordingly. Since the earth rotates, the sun appears to move at any time, hence the altitude and azimuth change with time.

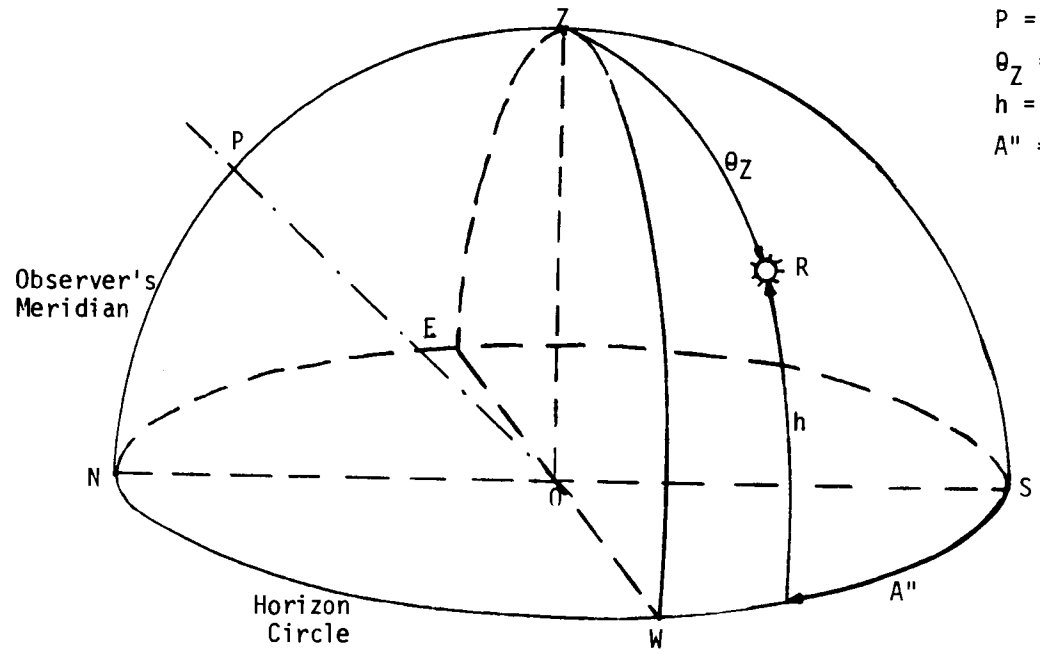

Z = zenith
O = origin (earth)
R = sun
P = north celestial pole
θ_Z = zenith angle = 90 - h
h = altitude
A" = azimuth

MASSACHUSETTS INSTITUTE OF TECHNOLOGY
SCHOOL OF CHEMICAL ENGINEERING PRACTICE
AT
OAK RIDGE NATIONAL LABORATORY

HORIZON SYSTEM OF COORDINATES

DATE	DRAWN BY	FILE NO.	FIG.
5-22-74	JSN	CEPS-X-192	1

There is a need for a coordinate system which will describe the sun's location on the celestial sphere relative to a fixed reference frame - the equator system of coordinates (1) (see Fig. 2). Extending the terrestrial equator to the celestial sphere constitutes a great circle, the celestial equator. Location of the sun is possible by means of an hour circle which passes from the celestial equator through the sun and intersects the celestial sphere at the north celestial pole. The angular distance measured along the hour circle from the celestial equator to the sun is the declination of the sun (δ). The right ascension of the sun (R.A.) is that distance measured from the vernal equinox (Γ) eastward along the celestial equator to the foot of the hour circle. Since these coordinates (δ, R.A., and Γ) refer to an origin on the celestial sphere, they are independent of an observer's position on earth. Also any effect of the earth's rotation is nullified since these coordinates rotate along with the earth. Therefore, δ and the R.A. remain essentially constant for a day. These solar coordinates change seasonally, however, due to the inclination of the ecliptic path of the sun (23.5° with the celestial equator plane).

Included within this picture is the semilocal coordinate system consisting of the declination and local hour angle (ω) of the sun. The parameter ω is defined as the angular distance measured from the observer's meridian along the celestial equator to the foot of the hour circle which passes through the sun and the north celestial pole (see Fig. 2). Solar noon [=1:36 pm (EDT) in Oak Ridge] corresponds to a local hour angle equal to zero (i.e., the sun is located on the observer's meridian). The latitude (Φ) given as arc ZD on Fig. 2 is that angle between an extended ZO line intersecting the terrestrial equator (EDW).

Figure 3 includes the horizon circle NESW, the observer's meridian NPZS, the celestial equator EDW, hour circle PRG, and the daily path of the sun during the summer CUF parallel to the celestial equator a constant angular distance δ degrees apart. Placing the collector on the east-west axis and hypothetically extending the collector surfaces through the sun and to the celestial sphere (EHW) constitute perfect alignment of the collector. Arc ZH is defined as the pointing angle $\S$ of the solar collectors. For perfect focusing, $\S$ [a function of Φ, δ, and ω (13)] varies continuously throughout the day (i.e., plane EHW intersects the sun on its path CUF at all times). For the purposes of this study the collectors are placed at a tilt angle β [$=\Phi - \delta$ (13)] given by arc ZU. The collectors are aligned using solar noon as the local hour angle. This means that perfect focusing is not always achieved and a pointing error Ψ [$=|\beta - \S|$ (13)] is introduced. Figure 4 shows the orientation of the parabolic reflector illustrating the tilt angle, pointing angle, and pointing error. Figure 5 depicts the pointing error as a function of local hour angle for May 14, 1974 (a test day) with the collector aligned with respect to solar noon. For Ψ greater than 4° a loss of solar incident radiation on the receiver (tube and fins) of the parabolic collector is significant (>15%) (13). From Fig. 5 a pointing error of 4° corresponds to about 10:30 am and 4:30 pm for May 14, 1974. At a 10° pointing error the parabolic collector receives no radiation from the reflecting surface and acts only as a flat plate collector receiving direct and diffuse radiation on the receiver (13). A 10° pointing error occurred at about 10:00 am and 5:00 pm on May 14, 1974. Details of the pointing error and angle calculations are presented in the previous MIT study (13).

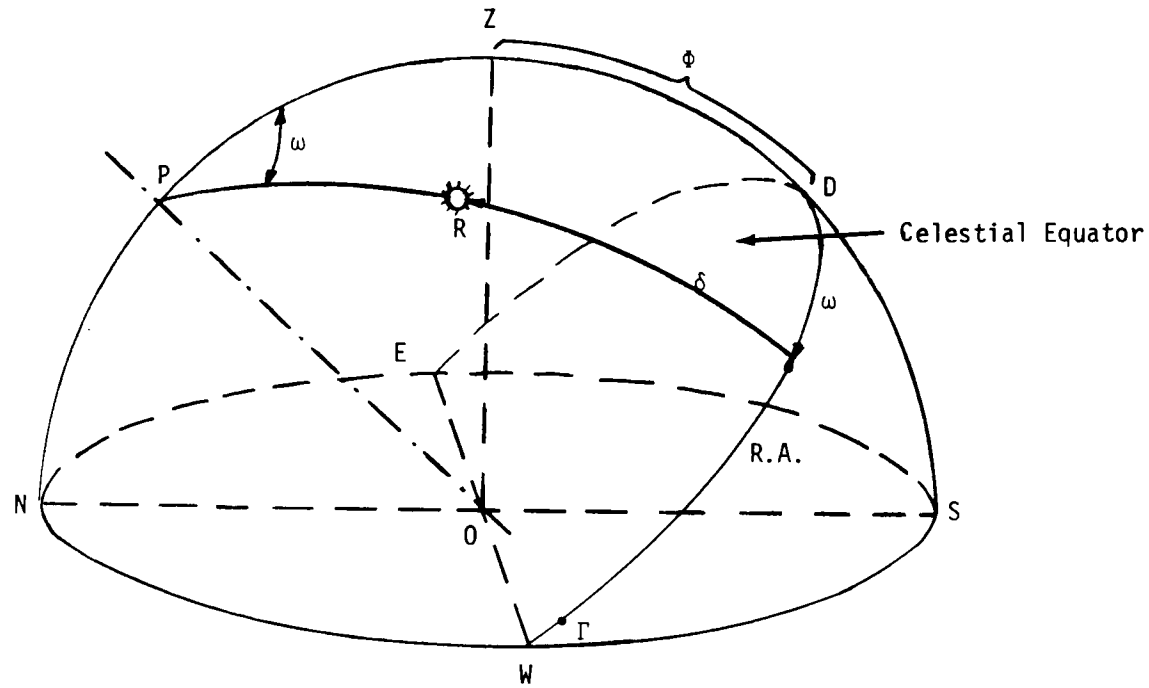

Γ = vernal equinox
δ = solar declination
Φ = latitude
R.A. = right ascension
ω = hour angle
(see Fig. 1 also)

MASSACHUSETTS INSTITUTE OF TECHNOLOGY
SCHOOL OF CHEMICAL ENGINEERING PRACTICE
AT
OAK RIDGE NATIONAL LABORATORY

EQUATOR SYSTEM OF COORDINATES

DATE	DRAWN BY	FILE NO.	FIG.
4-22-74	JSN	CEPS-X-192	2

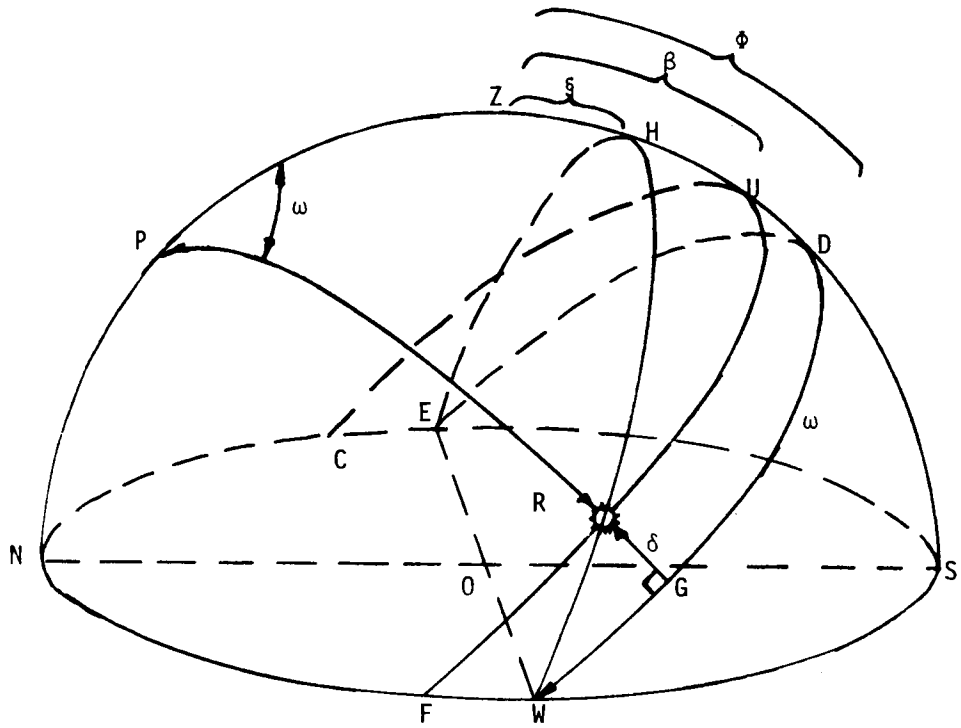

EDW = celestial equator
CUF = daily sun path
EHW = pointing angle focusing plane
Φ = latitude
β = tilt angle of collector
§ = pointing angle
δ = solar declination

MASSACHUSETTS INSTITUTE OF TECHNOLOGY
SCHOOL OF CHEMICAL ENGINEERING PRACTICE
AT
OAK RIDGE NATIONAL LABORATORY

POINTING ANGLE §

DATE	DRAWN BY	FILE NO.	FIG.
5-22-74	JSN	CEPS-X-192	3

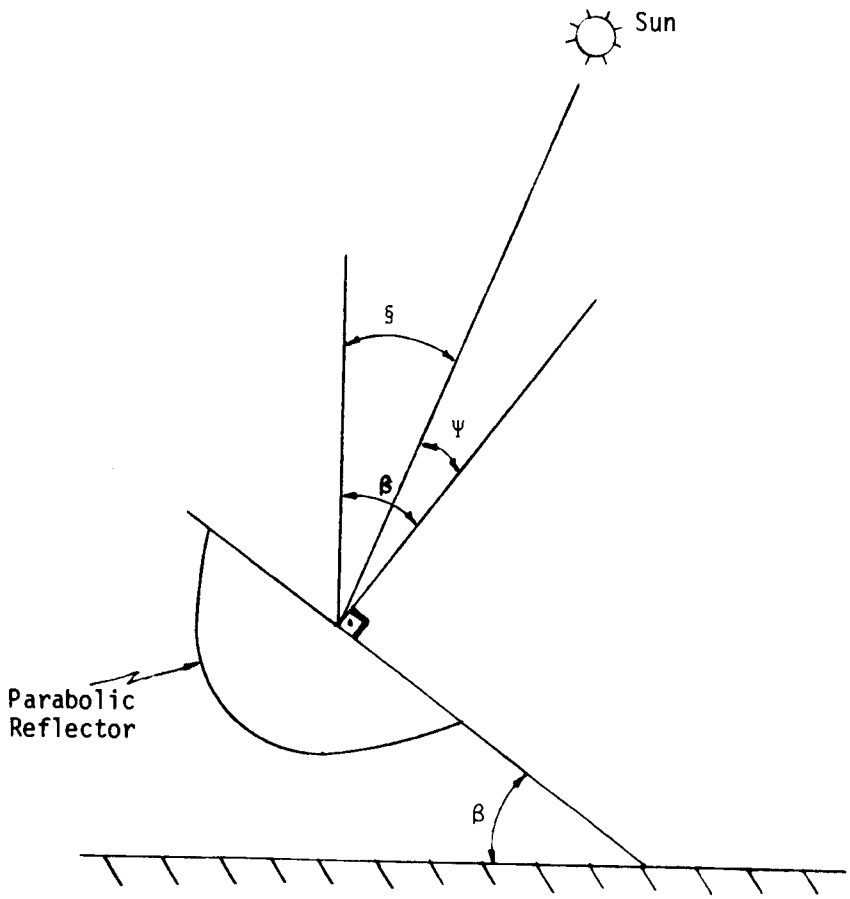

Reflector Aligned East-West

β = tilt of parabolic collector

§ = pointing angle of the sun

Ψ = pointing error = |β - §|

MASSACHUSETTS INSTITUTE OF TECHNOLOGY SCHOOL OF CHEMICAL ENGINEERING PRACTICE AT OAK RIDGE NATIONAL LABORATORY			
PARABOLIC COLLECTOR ALIGNMENT WITH POINTING ERROR			
DATE 5-24-74	DRAWN BY RDO	FILE NO. CEPS-X-192	FIG. 4

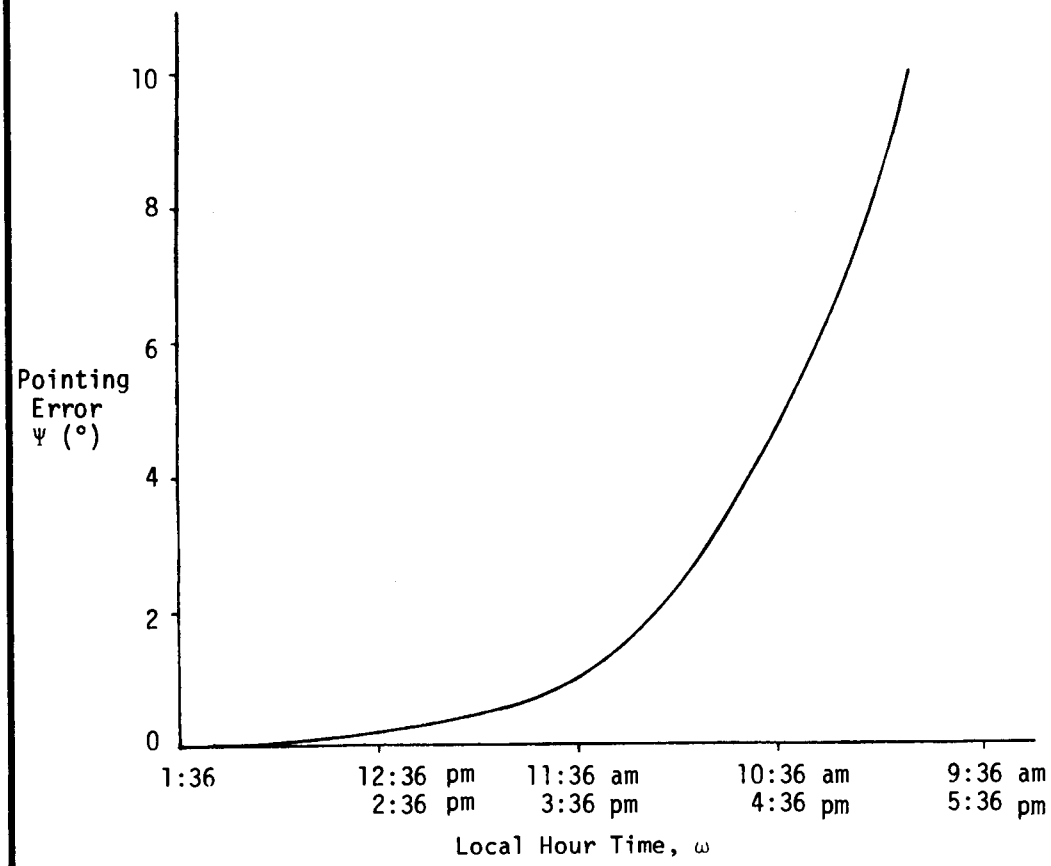

$\beta = 17.8°$

$\Phi = 36.0°$

$\delta = 18.2°$

MASSACHUSETTS INSTITUTE OF TECHNOLOGY
SCHOOL OF CHEMICAL ENGINEERING PRACTICE
AT
OAK RIDGE NATIONAL LABORATORY

POINTING ERROR AS A FUNCTION OF TIME FOR MAY 14, 1974

DATE	DRAWN BY	FILE NO.	FIG.
5-24-74	RDO	CEPS-X-192	5

4. THEORETICAL CHARACTERISTICS OF FINNED TUBE PERFORMANCE

The finned surface of the receiver for the parabolic collector is used to extend the interception area from the focal line to allow for pointing errors. Alternate ways of increasing the receiver interception area would be to:

1. increase the size of the fins. This would allow operation at larger pointing errors but would have two disadvantages in that the surface area for heat losses would be increased and the fin efficiency would be obviously less than with smaller fins.

2. increase the size of the tube. This, however, would introduce an unfavorable high thermal inertia into the system.

3. encase a larger tube with an evacuated glass (or similar material) cylinder to decrease heat losses and transients. However, material costs would be higher.

4. place a secondary reflector above the tube. This may be a viable alternative to the finned tube but would introduce additional costs.

5. use a rectangular, elliptical, or annular cross-section receiver to increase interception area while minimizing increases in thermal inertia. Again increased costs would have to be considered.

The characterization of the fin surface is paramount in determining the optimal performance of the finned tube. The effectiveness of the fin in transferring heat to the tube, and correspondingly to the working fluid, is essentially a function of its dimensions, thermal properties (i.e., conductivity and emissivity), the angle of tilt β of the reflector, and the inside tube heat transfer coefficient. The optimum fin length is a compromise between increased interception area and higher heat losses, while the importance of the material and its thermal properties can be expressed as a function of material cost economics. A previous MIT study (13) estimated the optimal alignment for periods of high insolation by estimating the solution to the fin equation through the introduction of a weighting factor which takes into account the increase in heat losses as the reflected light reaches the fin farther and farther away from the tube wall. The results indicated that for a day in March (near the vernal equinox) an alignment 2 to 3 hr before or after solar noon gave the largest amount of collected radiation for a constant tilt angle. However, to evaluate the useful heat input to the working fluid contained in the finned tube as a function of pointing error, the steady state fin equation must be solved for the distributed solar radiation flux F(y) along the finned surface (see Appendices 10.4.1 and 10.4.2):

$$\frac{d^2T}{dy^2} - \frac{2h_{eff}L_t(T - T_\infty)}{kA_f} + \frac{L_tF(y)}{kA_f} = 0 \qquad (1)$$

The variable y was used to indicate unidirectional transport along a vertically mounted fin.

Figure 6 indicates the relative intensity distribution on the fin for a 5° pointing error. A 5° pointing error was selected because it is near the maximum error that can be tolerated by the parabolic system and still obtain reasonable efficiencies (13). The energy density at any point on the fin is given by the incident radiation times a concentration factor (see Appendix 10.4.4). If the energy distribution for any given time and pointing error is known, the temperature distribution along the fin can be determined (see Appendices 10.4.3 and 10.4.4). Figure 7 illustrates a temperature distribution corresponding to a 5° pointing error, incident radiation of 250 Btu/ft^2-hr, and a working fluid temperature between 109 (T_{in}) and 166 (T_{out})°F. [It should be noted that the large temperature drop across the wall from 190°F to the log mean average fluid temperature of 136°F is due to the large fouling (the limiting resistance) observed in the galvanized steel pipe used for the tube in this study.] The useful heat input to the tube can then be evaluated at y = 0, the tube wall as:

$$q_u = kA \left.\frac{dT}{dy}\right|_{y=0} \tag{2}$$

which gives a quantitative measure of the effectiveness of the fin, or essentially its efficiency. The fin efficiency can then be defined as the ratio of the heat actually transferred from the fin to the tube to the heat that would be ideally transferred if the tube received the entire energy incident on the finned surface. The fin efficiency could also be expressed as an effectiveness of the fin surface relative to a similar fin of infinite thermal conductivity. In both cases the primary concern is with conduction heat losses as the solar energy distribution moves out from the tube along the fin and with minimization of the temperature gradient along the fin.

5. APPARATUS AND PROCEDURE

5.1 Apparatus

The apparatus (shown in Fig. 8) consisted essentially of:

1. a cylindrical (18.5 x 90 in. based on aperture area) parabolic collector and a finned tube receiver (1.92 x 90 in.) which was coated with flat black paint (absorptivity ∿0.87, emissivity ∿0.87) and placed along the focal line of the reflector. The collector was housed in a glass covered box insulated (1.25 in. thick) with fiberglass. The collector/receiver was used previously and has been described in detail (13).

2. a flat plate collector formed from a roll-bonded 17 x 50 in. aluminum plate with six parallel channels (∿15.26 in.^{3}, 250 cm^3 capacity) for water flow. The plate was coated with flat black paint (absorptivity ∿0.98,

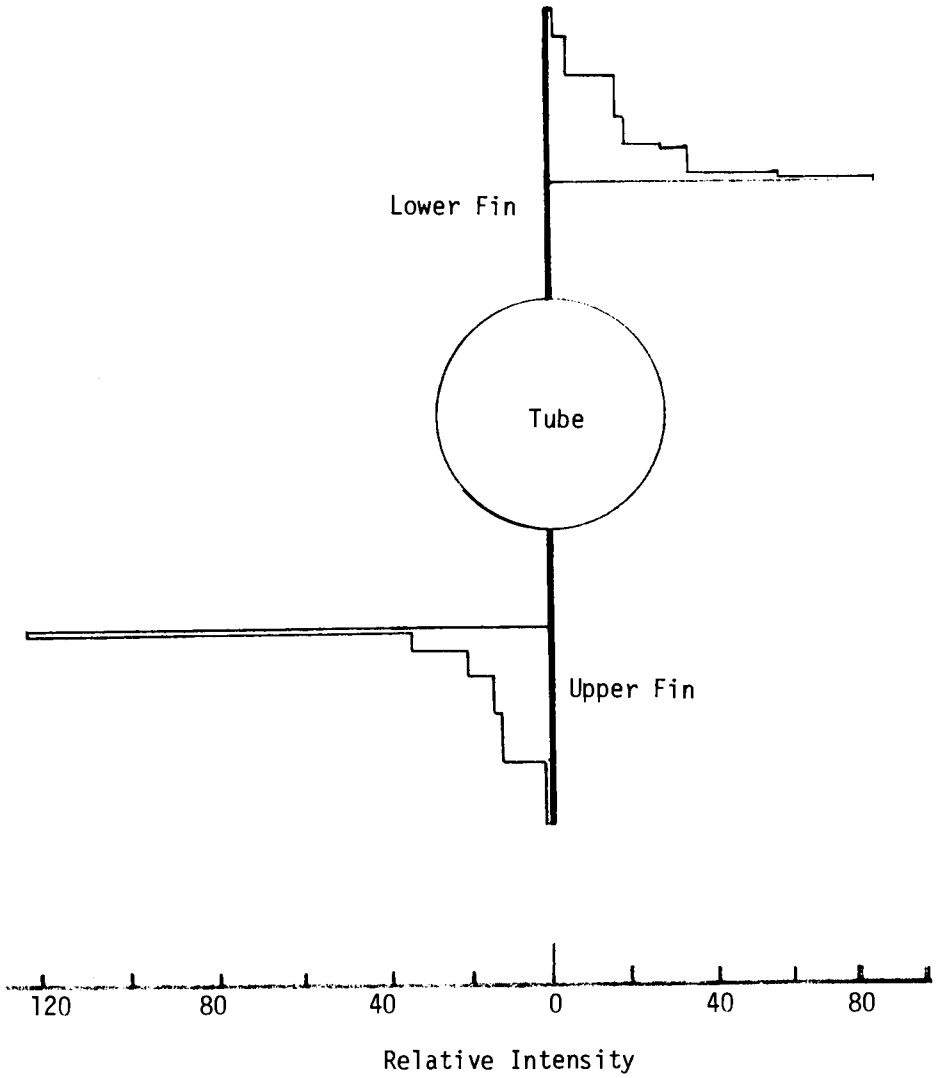

MASSACHUSETTS INSTITUTE OF TECHNOLOGY
SCHOOL OF CHEMICAL ENGINEERING PRACTICE
AT
OAK RIDGE NATIONAL LABORATORY

ENERGY DISTRIBUTION ON
FINNED TUBE FOR 5° POINTING ERROR
(RELATIVE INTENSITY)

DATE	DRAWN BY	FILE NO.	FIG.
5-20-74	JSN	CEPS-X-192	6

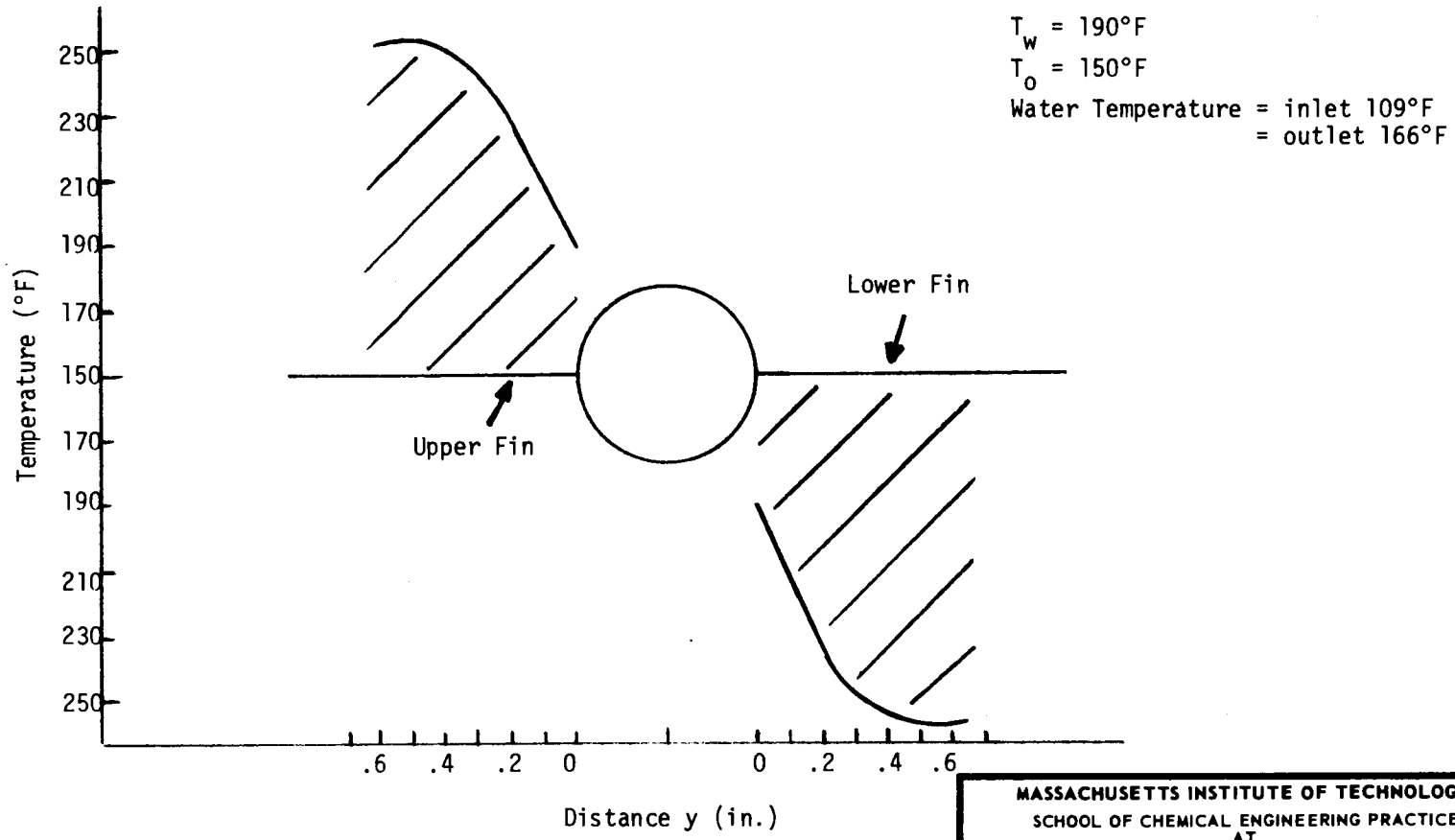

MASSACHUSETTS INSTITUTE OF TECHNOLOGY
SCHOOL OF CHEMICAL ENGINEERING PRACTICE
AT
OAK RIDGE NATIONAL LABORATORY

TEMPERATURE DISTRIBUTION ON FINNED TUBE FOR 5° POINTING ERROR

DATE	DRAWN BY	FILE NO.	FIG.
7-4-74	RMM	CEPS-X-192	7

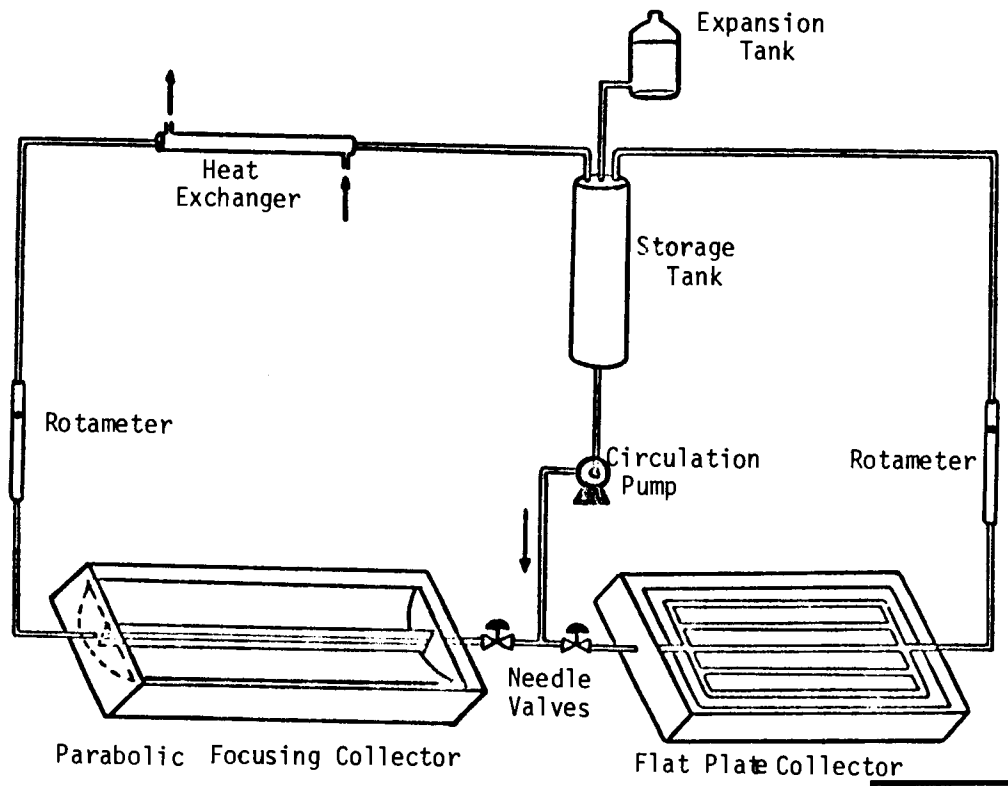

MASSACHUSETTS INSTITUTE OF TECHNOLOGY
SCHOOL OF CHEMICAL ENGINEERING PRACTICE
AT
OAK RIDGE NATIONAL LABORATORY

SCHEMATIC OF
EXPERIMENTAL APPARATUS

DATE	DRAWN BY	FILE NO.	FIG.
5-22-74		CEPS-X-192	8

emissivity ∿0.98) and housed in a 0.75-in.-thick plywood box lined with 5-in.-thick fiberglass insulation.

The box was fitted at the top with glass cover plates. Tap water was pumped from a steel storage tank simultaneously through the parabolic mirror receiver and the flat plate. A vented polyethylene tank was connected to the storage tank to allow for thermal expansion of the water. The inlet side of each collector was equipped with a needle valve to separately regulate the water flow rates. Rotameters were installed on the outlet side of each collector. A shell (galvanized steel) and tube (copper) heat exchanger was located between the rotameter for the parabolic collector and the storage tank to control the inlet water temperature to the collector. All piping connections were of fiberglass insulated heavy wall 0.5-in.-bore rubber hose. Materials were selected to place the system on a comparative economic basis with conventional home heating systems. Complete dimensions and properties of the materials used are presented in Appendix 10.6.

Temperatures were measured by means of twenty-four 18-22 gauge chromel-alumel thermocouples connected to two Honeywell-Brown electronic 12-channel printing recorders (0-500°F) (See Tables 1 and 2 for thermocouple locations). Two National Bureau of Standards calibrated Eppley pyrheliometers were used to measure diffuse and total radiation, the difference in intensities giving the direct radiation on a horizontal surface. An Esterline-Angus graphic ammeter connected to an Electrolet Killark FSC-3 anemometer was used to measure wind velocity in the vicinity of the collectors.

5.2 Procedure

The two collectors were operated simultaneously under the following operating and design conditions:

1. Nominal outlet water temperatures of 135, 165, and 185°F.

2. One and two glass cover plates, 0.25 and 0.5-in. spacing.

3. Orientation of collector.

A quasi-steady state period was defined when the outlet temperature could be maintained (by adjusting the flow rates) to within ±5°F of the nominal value for approximately 15 min. Inlet water temperatures were kept constant within 1°F for each run by adjusting the cooling water flow rate through the heat exchanger. The parabolic collector was focused once each hour for all but the early set of test runs (May 5-7). The thermocouples were calibrated with a potentiometer and an ice junction and were found to vary ±1°F from the recorder reading. The flow rate measurements were corrected for viscosity changes using correlations between the flow coefficient and the viscous influence number for the individual rotameters (6). These corrections become significant above room temperature. Flow rate measurements at specific temperatures agreed with predicted flow rates to within 3% (the accuracy of the flow rate measurements).

Table 1. Thermocouple Locations - Flat Plate Collector

Flat Plate Recorder (No. 1) Channel No.	Thermocouple No.	Location
1	1	inlet water
2	2	outlet water
3	3	underside panel center
4	4	outside panel center
5	5	under insulation panel center
6	6	center panel edge
7	7	underside center on water channel
8	8	corner edge of panel downstream
9	9	corner edge of panel upstream
10	10	air space above panel
11	11	outer surface of glass plate
12	12	underside box center

Table 2. Thermocouple Locations - Parabolic Collector

Flat Plate Recorder (No. 2) Channel No.	Thermocouple No.	Location
1	1	middle of box, under insulation, 6 in. from end
2	2	center of underside of reflector, 6 in. from tank
3	3	center of underside of reflector, 2 ft from tank
4	4	end of finned tube (tank side)
5	5	middle of finned tube
6	6	end of finned tube (away from tank)
7	14	fin (center of tube)
8	16	inside of glass cover plate
9	15	outside of glass cover plate
10	17	ambient
11	11	water inlet to receiver
12	12	water outlet from receiver

6. RESULTS AND DISCUSSION

6.1 Experimental Results

Results from fifteen experiments are presented in Table 3. The terms used are:

Time = date, time, and duration of experiment

T_O = ambient temperature

$T_{out,av}$, $T_{in,av}$ = measured average outlet and inlet water temperatures

ΔT_{av} = average measured temperature rise of working fluid

H_{TOT}, H_{DIF} = total and diffuse insolation falling on a horizontal surface

$R_D(H_{TOT} - H_{DIF})$ = direct insolation corrected for collector orientation (see Sect. 3)

$H_S = (R_S H_{DIF})$ = diffuse insolation corrected for collector orientation (see Sect. 3)

H_T = total insolation corrected for collector orientation

$q_u)_{EXP/A}$ = observed output of useful heat per square foot of receiver surface (flat plate area or aperture area)

Eff_{OBS} % = observed collector efficiency = $q_u)_{EXP}/H_T$

Conditions = weather conditions, orientation, number of layers of glass

Additional temperature data are available in Appendix 10.8; the values presented here were those used for heat loss and efficiency calculations. While outlet and inlet temperatures were held relatively constant during any one experiment, insufficient cooling capacity led to a steady rise in the inlet water temperature throughout each day. The temperature drop exhibited by Run 12 occurred when cold water was added to the system.

Solar insolation (H_{TOT},H_{DIF}) was calculated by planimeter integration of pyrheliometer records covering the period of each experiment. Observed useful heat, $q_u)_{EXPT}$, was determined from the temperature rise and mass flow rate of the working fluid (water). It should be noted that the area of the flat plate collector is 51% that of the parabolic collector; thus $q_u)_{EXPT}$ values for the flat plate are expected to be lower than those of the parabolic collector.

The experiments were performed under a variety of sky conditions. Runs 1 and 2 were performed on a heavily overcast day which prevented attainment of any significant ΔT across either unit. Runs 4, 5, 7, and 8 were performed

TABLE 3. EXPERIMENTAL RESULTS

			Flat Plate Collector									Parabolic Focusing Collector							
Run	Time Interval	Conditions	$(T'_{in})_{av}$ (°F)	$(T'_{out})_{av}$ (°F)	$(\Delta T)'_{av}$ (°F)	T_o Ambient (°F)	$R'_D(H_{TOT}-H_{DIF})=H'_D$ (Btu/ft^2)	$R'_S H_{DIF}=H'_S$ (Btu/ft^2)	H'_T (Btu/ft^2)	$(q_u)'_{EXP}/A'$ (Btu/ft^2-hr)	$(Eff)'_{OBS}$ (%)	$(T_{in})_{av}$ (°F)	$(T_{out})_{av}$ (°F)	$(\Delta T)_{av}$ (°F)	$R_D(H_{TOT}-H_{DIF})$ (Btu/ft^2)	$R_S(H_{DIF})$ (Btu/ft^2)	H_T (Btu/ft^2)	$(q_u)_{EXP}/A$ (Btu/ft^2-hr)	$(Eff)_{OBS}$ (%)
3	5-7-74 11:36-11:49	very clear 1 plate	80	186	106	67	55.65	6.58	62.23	75.0	26	83	182	99	55.7	6.64	62.34	136.35	47
6	5-8-74 12:23-12:39	clear with haze 2 plates, ¼ in. spacing	92	157	65	77	62.82	16.46	79.28	184.32	62	93	162	69	62.76	16.49	79.25	132.1	44
9	5-13-74 12:00-12:16	clear with haze 1 plate for the parabolic and 2 plates for the flat plate ½ in. spacing	108	167	59	75	55.43	25.46	80.89	163.98	53	109	166	57	55.43	25.51	80.94	98.51	32
10	14:28-14:55		117	185	68	80	100.85	31.75	132.6	155.56	53	117	184	67	101.04	31.82	132.86	120.4	41
11	15:05-15:41		122	166	44	83	134.78	33.40	168.18	143.50	51	121	165	44	134.91	33.57	168.48	86.13	30
12	16:34-16:59		106	134	28	87	76.32	12.58	88.9	133.02	61	102	132	30	77.32	12.80	90.12	37.83	17
13	5-14-74 10:23-10:55	very clear	85	135	50	72	102.71	18.59	121.3	129.03	56	84	138	54	103.94	18.87	122.81	63.95	28
14	11:35-12:09	parabolic one plate	96	167	71	79	151.03	17.96	168.99	182.15	60	96	166	70	150.88	17.90	168.78	113.99	38
15	13:10-13:30	flat plate 2 plates ½ in. spacing	108	185	77	82	96.09	9.37	105.46	167.29	52	108	185	77	95.91	9.30	105.21	129.97	41
16	15:20-15:42		123	163	40	88	92.22	10.64	102.86	175.65	62	121	164	43	92.22	10.64	102.86	95.37	34

under intermittent cloud conditions which made attainment of quasi-steady state operation extremely difficult due to the control limitations of our apparatus. The installation of thermostats and recording flowmeters could have eliminated this problem, but time limitations prevented such modifications.

Observed efficiencies indicate that for the relatively low operating temperature range of the tests the flat plate covered with two layers of glass consistently out-performed the parabolic collector provided with one layer of glass (Runs 9-16). When both units were supplied with one layer of glass, the flat plate efficiency was considerably less than that of the parabolic collector, 26% versus 47% (Run 3). The addition of a second layer of glass plates to both units increased the efficiency of the flat plate unit dramatically relative to the parabolic collector (61% for the flat plate vs 44% for the parabolic). Although the two experiments are not directly comparable due to the different operating temperatures, the effect observed indicated that the addition of a second layer of glass significantly lowers the heat losses from the flat plate while leaving the parabolic collector's heat losses relatively unchanged.

It should be noted that the experiments performed were limited to relatively low temperatures because the system operated at atmospheric pressure and was prone to severe flow rate fluctuations above 185°F, presumably due to boiling at hot spots in both receivers. These low temperatures favored the operation of the flat plate collector as was demonstrated by an experiment performed on May 8 in which both units were allowed to equilibrate with no working fluid in the receivers. The flat plate reached temperatures of 250°F while the receiver in the parabolic collector reached equilibrium at 340°F. This indicates that the parabolic collector would be capable of sustaining a finite flow rate at 250°F while the flat plate collector would not. At a 250°F operating temperature [used by Fraas (6) for the operation of a LiBr absorption cooling system] the parabolic reflector would therefore be the preferred collector design.

Operation of both units at higher temperatures would be of interest. The existing apparatus has been shown capable of maintaining the 15 psi pressure required to operate in the area of 250°F. An evaluation of the effect of a second layer of glass on the parabolic receiver should also be performed at the higher operating temperatures where additional reductions in heat losses would be desirable.

Experiments were carried out on dates (5/8-5/14) when the sun was approaching the summer solstice, hence pointing errors were relatively large despite orientation adjustments. Optimal performance was not, therefore, achieved for either unit.

Efficiencies observed for the flat plate collector were comparable to those observed by Hottel (10). Efficiencies observed by Löf (11, 12) for the cylindrical parabolic were somewhat higher. In comparing the equipment used in this study with that used by Löf and his coworkers, there are several important differences which can account for the lower efficiencies observed. The finned tube receiver used was far from an optimum design. A large

temperature gradient existed along the fin (fin efficiency $\ll$ 100%), and there was a considerable amount of fouling in the tube itself. Our system of a fixed parabolic collector with periodic focusing differs from Löf's device which was kept in alignment at all times by tracking. For our lower concentration factor (9.8) device, insulation of the containment enclosure was important in maintaining high efficiencies. In future experiments, more insulation and an improved receiver will be used.

6.2 Comparison Between Observed and Theoretical Useful Heat Gained by Working Fluid for the Flat Plate and Parabolic Focusing Solar Energy Collectors

The total solar energy absorbed by the flat plate and parabolic focusing collectors, Q_A' and Q_A (Btu), respectively, is distributed among three sections of each collector:

1. Useful heat absorbed by the working fluid, q_u (Btu/hr).

2. Convective and radiative thermal losses from the collector surface to the glass plate(s) above and out to the atmosphere, q_G.

3. Conduction and convective thermal losses from behind the collector surface through the insulation, wood, and out to the atmosphere, q_B.

A theoretical q_u is determined by evaluating q_A and subtracting the sum of the thermal losses q_G and q_B. By monitoring the flow rate and inlet and outlet temperatures of the working fluid, an experimental q_u is calculated. Knowing the time duration Δt of a quasi-steady state run allows for the determination of total energy quantities ($Q = q\Delta t$). A detailed qualitative and quantitative discussion of these important performance variables is given in Appendices 10.1 and 10.2.

Table 4 lists the theoretical and experimental Q_u for each quasi-steady state run obtained for both solar collectors. Also tabulated are the thermal losses through the glass (Q_G) and box (Q_B). Values for theoretical and experimental useful heats are generally in good agreement.

For the flat plate collector using two glass plates the minimum and maximum disagreement between theoretical and experimental Q_u' are 14 and 41% corresponding to Runs 14 and 10. The theoretical Q_u' is less than the observed Q_u' for each quasi-steady state run. Thermal losses through the glass (Q_G') and losses through the wood and insulation (Q_B') account for about 40 and 3% of the total energy absorbed by the collector plate.

Comparison of theoretical and experimental Q_u for the parabolic focusing collector using one glass plate shows a minimum and maximum disagreement of 2% and 43%, corresponding to Runs 10 and 14. With the exception of Runs 12 and 14, theoretical Q_u values are less than the observed values. These differences are caused by focusing misalignment and shading effects due to the position of the sun at these quasi-steady state times. Run 12 was observed between 4:34 and 4:59 pm, greater than three hours from solar noon. Thermal

Table 4. Comparison Between Observed and Calculated Useful Heat Gain

Run	Date	No. of Glass Plates n'	Observed Total Energy Absorbed by Plate (Btu) Q_A	Calculated: Energy Lost by Plate Through Glass (Btu) Q_G	Calculated: Energy Lost by Plate Through Box (Btu) Q_B	Calculated: Useful Energy Gained by Working Fluid (Btu) Q_u'	Observed Energy Gained by Working Fluid (Btu) $(Q_u')_{EXPT}$	$(Q_u')_{EXPT}$ minus Q_u' (Btu)	Disagreement % Error	Experimental Efficiency (%) $(Eff')_{EXPT}$	Atmospheric Temperature (°F) T_o	Inlet Working Fluid Temperature (°F) T_{in}'	Outlet Working Fluid Temperature (°F) T_{out}'
Flat Plate													
3	5-7	1	305	246	14	45	96	51	53	19	67	80	186
6	5-8	2	345	88	8	249	290	41	16	61	77	92	157
9	5-13	2	344	115	11	218	258	40	16	53	75	108	167
10	5-13	2	574	304	26	244	413	169	41	53	80	107	185
11	5-13	2	731	345	30	356	508	152	30	51	83	122	166
12	5-13	2	360	94	10	256	327	71	22	61	87	106	134
13	5-14	2	503	144	14	345	406	61	15	56	72	85	135
14	5-14	2	751	222	19	510	609	99	14	60	79	96	167
15	5-14	2	476	184	16	276	329	53	16	52	82	108	185
16	5-14	2	449	136	12	301	380	79	21	62	88	123	163
Parabolic		n	Q_A	Q_G	Q_B	Q_u	$(Q_u)_{EXPT}$	$Q_u)_{EXPT}-Q_u$	% Error	$Eff)_{EXPT}$	T_o	T_{in}	T_{out}
3	5-7	1	619	228	96	295	343	48	14	47	67	83	182
6	5-8	2	635	*	155	*	409	-	-	44	77	93	162
9	5-13	1	570	209	123	238	305	67	19	32	75	109	166
10	5-13	1	1020	396	263	361	629	268	43	41	80	117	184
11	5-13	1	1367	492	335	540	600	60	10	30	83	121	165
12	5-13	1	695	205	252	238	183	-55	30	17	87	102	132
13	5-14	1	851	324	202	325	396	71	18	28	72	84	138
14	5-14	1	1511	469	277	765	750	-15	2	38	79	96	166
15	5-14	1	971	302	193	476	503	27	5	41	82	108	185
16	5-14	1	863	277	201	385	406	21	5	34	88	121	164

*Q_G could not be evaluated effectively due to insufficient data.

losses through the box (23% of Q_A) are less than losses through the glass (35% of Q_A) with the exception of Run 12 even though the overall surface areas differ only by a factor of 2.5 for the parabolic collector. Q_B is about eight times as great as Q_B'. The insulation thickness is 1.25 in. for the parabolic compared with 5 in. for the flat plate. Thus, it is recommended that more insulation be added behind the parabolic reflector to decrease heat loss through the box (see Appendix 10.1).

Run 3 was performed using just one glass plate for the flat plate collector. A heat loss through the glass accounted for 80% of the total absorbed energy by the plate. This corresponds to twice as much loss through the glass for the one glass plate system as for the two glass plate system. Run 6 was performed operating the parabolic collector with two glass plates. Because neither temperatures of the inner glass nor the air space temperature between the reflector and inner glass were observed, Q_G could not be calculated with sufficient accuracy.

6.3 Monthly Efficiencies for Oak Ridge Weather Conditions

To determine the feasibility of using a flat plate collector in Oak Ridge, further characterization of its efficiency throughout the year was made. The flat plate considered had specifications similar to the unit used in the present report. The efficiencies were calculated as the ratio of the useful energy collected to the total radiation incident on the collector.

The operating conditions considered were working fluid (water) outlet temperatures of 135, 165, and 185°F. The inlet temperature was assumed to be constant at 100°F, and the useful energy was estimated as the total energy absorbed (q_A') minus the heat losses ($q_G' + q_B'$).

The total radiation (incident on a horizontal surface) has been tabulated for the last 16 years for the Oak Ridge area by Gifford and Culkowski (4, 5). Daily averages for each day of the year for a period of 15 years were also available and monthly averages were determined (Fig. 9, Table 5). The direct and diffuse radiations were determined using the total radiation and Oak Ridge weather conditions (see Appendix 10.3 and Fig. 9).

Because of significant amounts of haze and turbidity, diffuse radiation for the months of May through October is higher than the direct radiation. The total direct and diffuse radiation values for each month were corrected for orientation of the collector (see Appendix 10.3.2, Table 8). Two angles of tilt were considered: Case 1 used a $\beta = 36°$, the latitude of Oak Ridge, for Case 2 $\beta = 51°$ favoring the winter solstice by 15°, which should improve the operating efficiencies in the winter months (10). A third case was developed in which the maximum efficiencies of the flat plate with $\beta = 36°$ were calculated using the 16 year average maximum total radiation for each month (zero sky cover). Calculated efficiencies of the flat plate used conditions as solar noon with two glass plates to reduce heat losses. The average temperature of the flat plate, T_{LM} (assumed constant through the

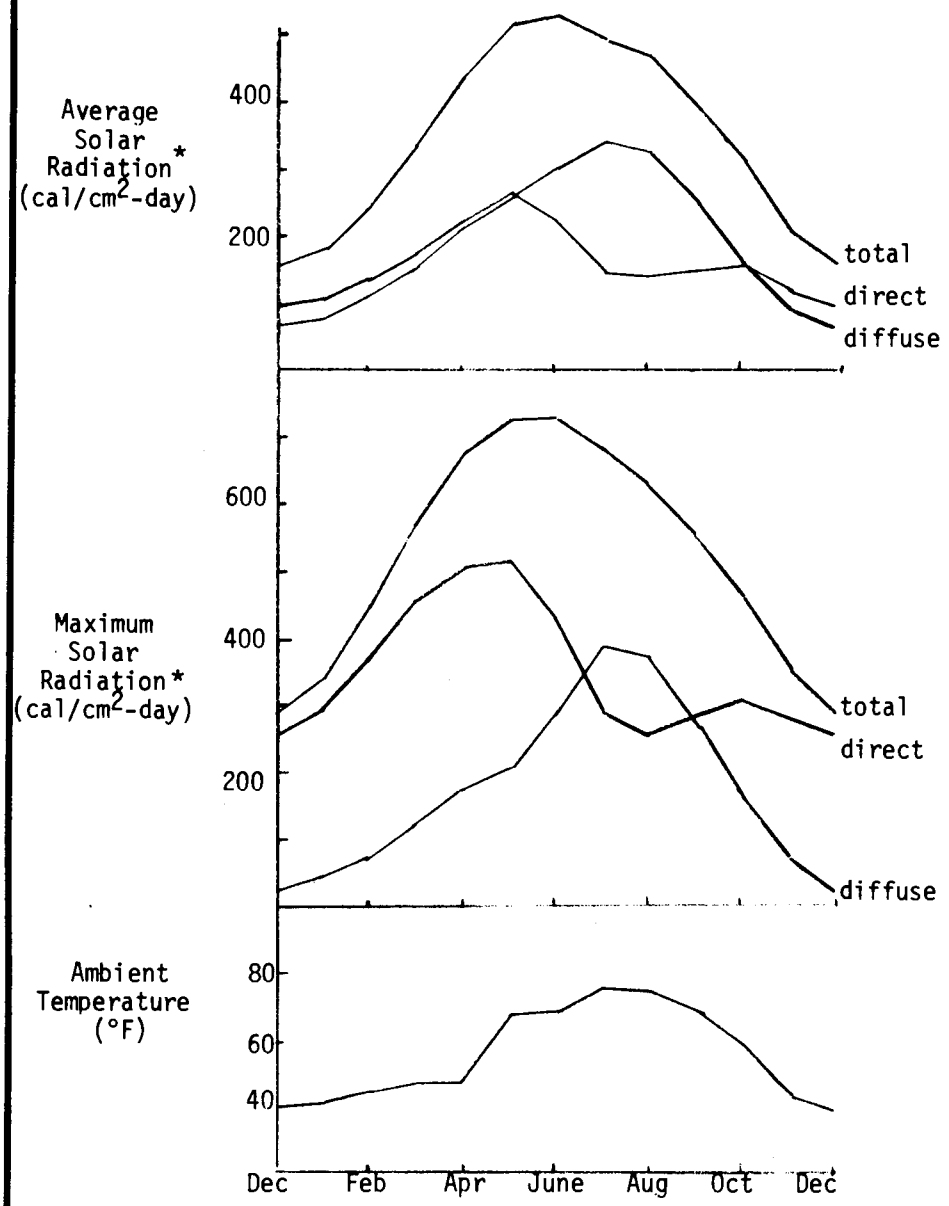

*Radiation Flux Incident on Pyrheliometer

1955-1971 (16 years used)

MASSACHUSETTS INSTITUTE OF TECHNOLOGY
SCHOOL OF CHEMICAL ENGINEERING PRACTICE
AT
OAK RIDGE NATIONAL LABORATORY

INSOLATION AND AMBIENT TEMPERATURES FOR OAK RIDGE

DATE	DRAWN BY	FILE NO.	FIG.
5-24-74	CD	CEPS-X-192	9

year), was equal to the log mean temperature difference of the inlet and outlet working fluid temperatures, i.e., 117, 130, and 138°F corresponding to the outlet temperatures of 135, 165, and 185°F, respectively.

For each case the energy absorbed and heat losses through the bottom of the box and through the glass were calculated using the above assumptions. Figures 10, 11, and 12 each consist of three plots: the average solar radiation flux vs time (for different months of the year), heat losses vs time, and the efficiency vs time (see Appendix 10.3.2). The plot of solar radiation flux incident on the collector vs time shows total radiation, direct radiation, and diffuse radiation versus time.

The incident heat flux versus time plots are identical since only the tilt angle and the radiation fluxes were changed, and in calculating the heat losses, only the plate temperature (assumed constant through the year) and the ambient temperature are needed. A constant average wind speed of 3 mph was also assumed.

The heat losses through the glass are represented with operating temperatures of 135, 165, and 185°F. Notice that the heat losses through the bottom of the box were very nearly equal in all three cases and are represented by the lower curve on the plot. The efficiency vs time plot presents the efficiency curves calculated for each outlet temperature.

Figure 10 presents the results from the first case in which it was assumed that the tilt angle was equal to the latitude (36°). From the solar radiation flux plot, the highest total radiation incident on the collector, 134 Btu/ft^2-hr, occurs during the month of May. From October through May the direct radiation is considerably higher than the diffuse, while during the months of June through September, diffuse radiation is more important.

The heat losses from the flat plate are at a minimum in July and August and a maximum in December and January. As expected, heat losses occurring at the high operating temperature (185°F) are higher than those occurring at the lower operating temperature. From the efficiency plot it is observed that the unit is operating more efficiently at low outlet temperatures. Under the assumptions made in calculating the efficiencies, i.e., the dimensions of the unit used in the experiments and average monthly solar radiation fluxes, the unit could not be operated during parts of December and January. It should be noted that while the average day during this time may be unsuitable for efficient collector operation, a properly designed system could operate on intermittent clear days and collect sufficient amounts of energy to provide heat until the next period of clear skies. (Case 3 discussed later illustrates the efficiencies obtained by assuming clear sky operation.) At the outlet temperature of 135°F, the unit's efficiency for the average day reaches its maximum, 34%, in May, June, and July at an operating temperature of 135°F. It reaches a maximum of 23.7%, but the unit cannot be operated on an average day during November, December, January, and February. For an operating temperature of 185°F the unit reaches maximum efficiency of 16% and cannot be operated on the average day from October until April.

Figure 11 is for the second case in which it was assumed that the tilt angle of the unit equaled the latitude +15° favoring the winter solstice.

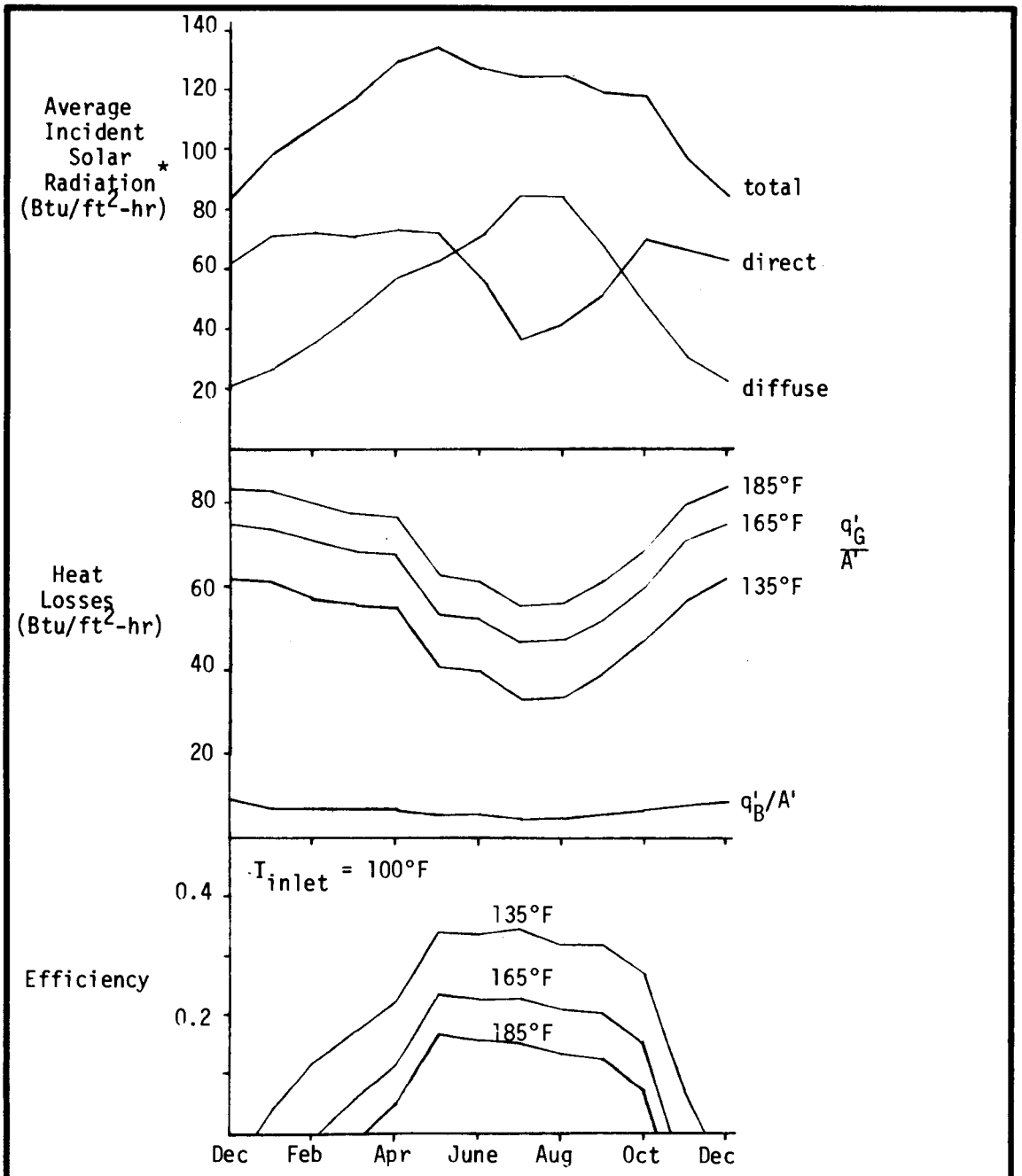

*Radiation Flux Incident on the Collector

MASSACHUSETTS INSTITUTE OF TECHNOLOGY
SCHOOL OF CHEMICAL ENGINEERING PRACTICE
AT
OAK RIDGE NATIONAL LABORATORY

PERFORMANCE VARIABLES FOR FLAT PLATE, CASE 1 (β = 36°)

DATE	DRAWN BY	FILE NO.	FIG.
5-20-74	CD	CEPS-X-192	10

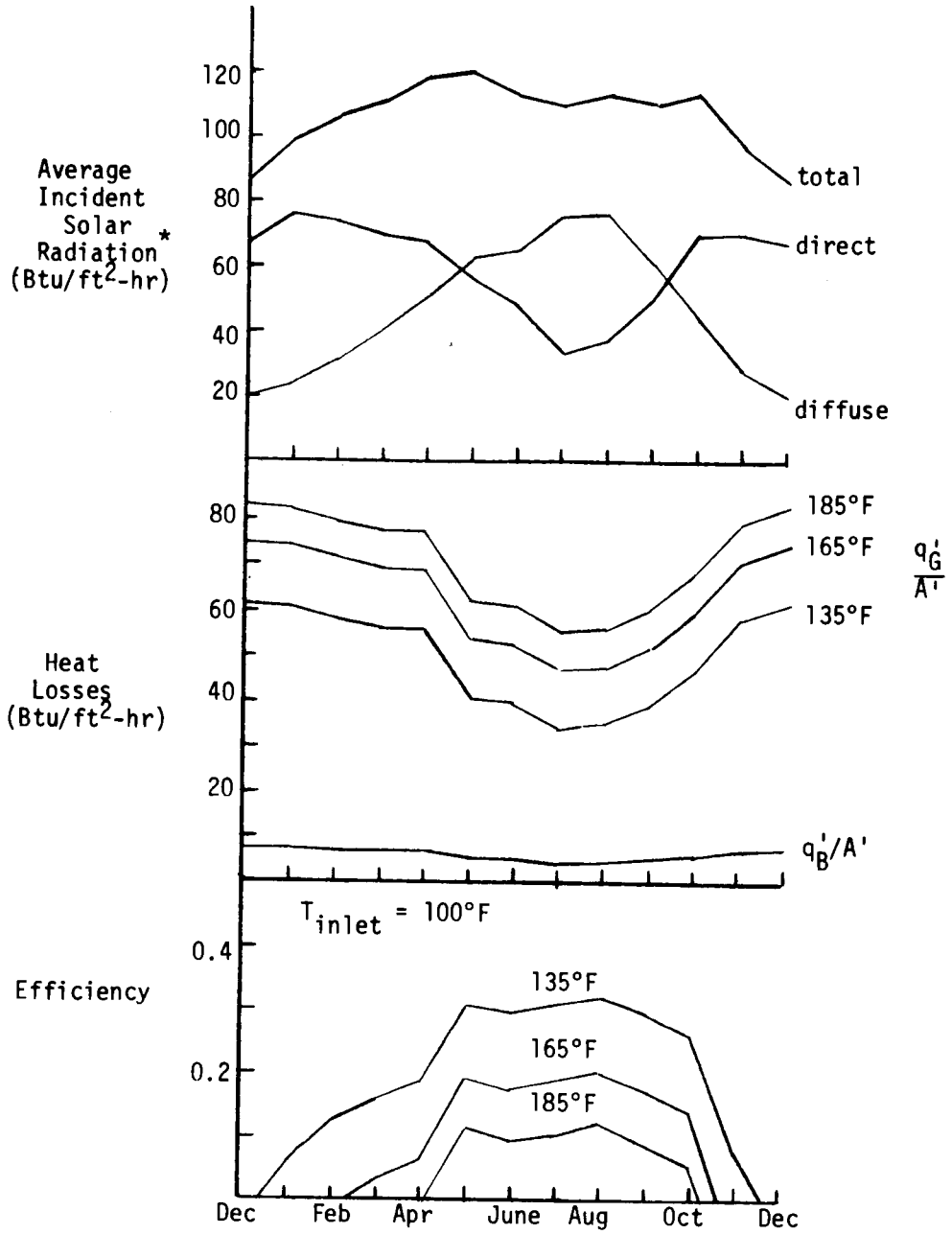

*Radiation Flux Incident on the Collector

MASSACHUSETTS INSTITUTE OF TECHNOLOGY
SCHOOL OF CHEMICAL ENGINEERING PRACTICE
AT
OAK RIDGE NATIONAL LABORATORY

PERFORMANCE VARIABLES FOR FLAT PLATE, CASE 2 (β = 51°)

DATE	DRAWN BY	FILE NO.	FIG.
5-23-74	EJK	CEPS-X-192	11

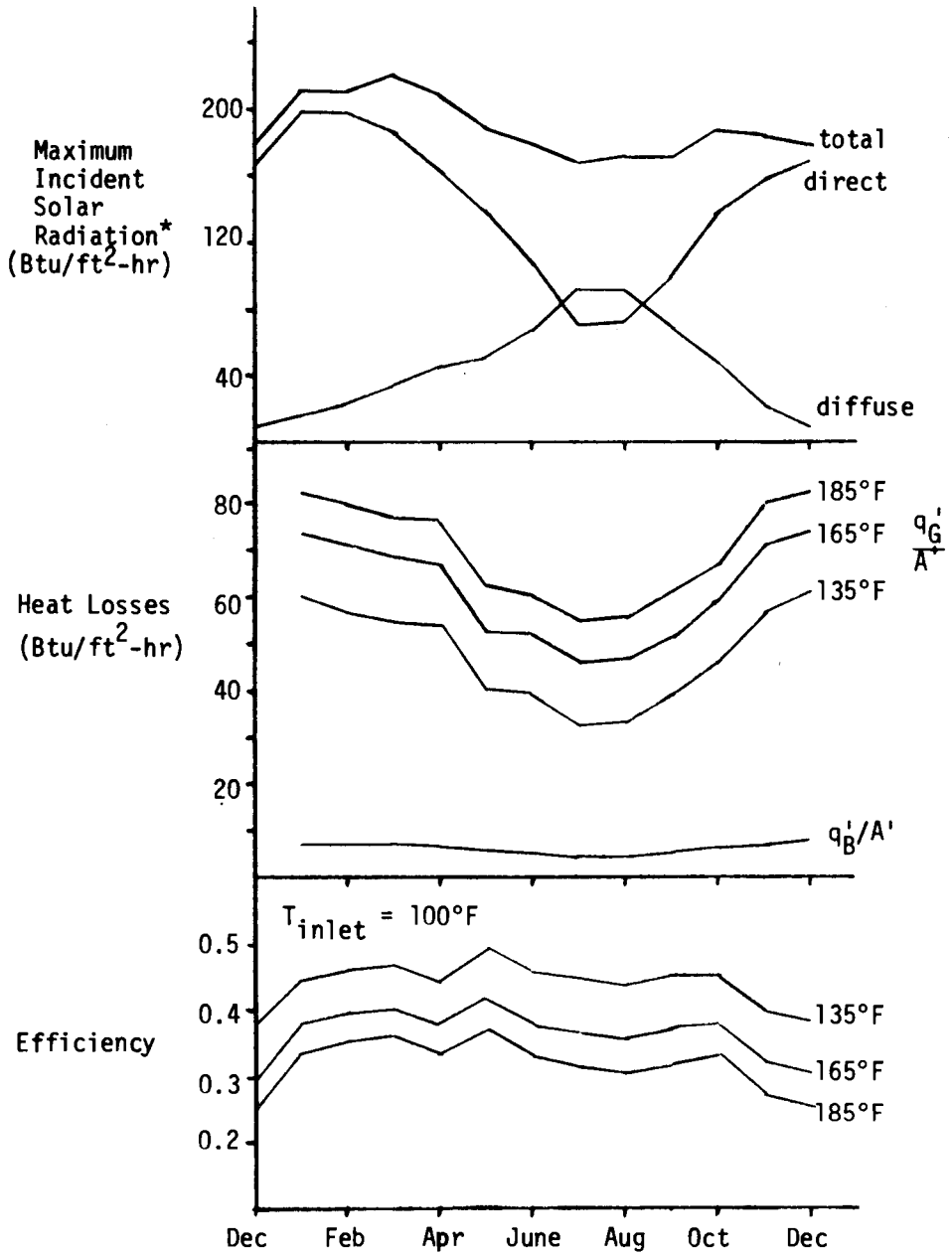

*Radiation Flux Incident on the Collector

MASSACHUSETTS INSTITUTE OF TECHNOLOGY
SCHOOL OF CHEMICAL ENGINEERING PRACTICE
AT
OAK RIDGE NATIONAL LABORATORY

PERFORMANCE VARIABLES FOR FLAT PLATE DURING MAXIMUM INSOLATION, CASE 3 (β = 36°)

DATE	DRAWN BY	FILE NO.	FIG.
5-21-74	CD	CEPS-X-192	12

The highest total radiation incident on the collector is 119 Btu/ft^2-hr for the month of May. The maximum efficiencies are 30.7, 19, and 12% for operating temperatures of 135, 165, and 185°F, respectively. Comparison of Cases 1 and 2 shows that the incident radiation for Case 1 is higher than for Case 2 except for December and January. This would mean that the efficiency for January and December would be higher but it would be lower during the remainder of the year. The calculated efficiency curves illustrate this effect. Improvements and reductions in the diffuse and direct insolation partially cancel for the months of December and January as both orientation factors (R_D and R_S) change differently as the tilt angle changes. In November and January the efficiencies for Case 2 will be higher by 1 and 2%, respectively, while for the rest of the year it will be lower by 1 to 4%.

For operating temperatures of 165 and 185°F, the efficiencies for Case 2 are much lower than the efficiencies for Case 1. Since for the operable months the solar radiation flux for Case 1 was higher than Case 2, it is concluded that the flat plate is best operated at a tilt angle of 36° (latitude) under the present assumptions.

Some days in each of the months throughout the year will have a high daily average solar radiation flux if there is no cloud (sky) cover. The efficiency of the unit for these days should represent optimum performance. Figure 12 illustrates the third case in which the total radiation reaches a maximum of 220 Btu/ft^2-hr in March. The direct radiation is considerably higher than the diffuse as the model assumed that atmospheric turbidity is the only contributing factor to diffuse radiation. The efficiencies are high for operating temperatures of 135, 165, and 185°F; maximum efficiencies of 50, 42, and 37%, respectively, occur in May.

To calculate the efficiency of the unit for those days in the winter months for which the average solar radiation and ambient temperature could be used, it would be necessary to take into consideration the number of days the unit could be operated. This would require a rigorous study for each day of the year, and a plot of frequency versus the ratio of the incoming energy absorbed to the total incoming energy. From this information the number of days the unit could operate during that month can be determined.

7. CONCLUSIONS

1. The flat plate collector covered with two layers of glass demonstrated higher experimental efficiencies than the cylindrical parabolic collector covered with one or two layers of glass while operating over the temperature range of 135 to 185°F under Oak Ridge weather conditions. This was expected because of: (1) reflector losses at the Alzak aluminum reflector (13%), (2) diffuse to total insolation levels as high as 40%, (3) differences in the fin efficiencies of the absorbing surfaces of both devices, and (4) differences in the amount of thermal insulation around the collector.

2. Oak Ridge weather conditions have been correlated in terms of monthly average and monthly maximum insolation (total, diffuse, direct).

3. The theoretical performance of the flat plate and cylindrical parabolic units have been characterized as functions of weather, design parameters, and operating conditions.

4. The performance model for the flat plate collector has been extended to allow prediction of average and optimal collector operation for each month of the year under Oak Ridge weather conditions.

5. The energy distribution on the finned tube receiver in the cylindrical parabolic reflector has been characterized as a function of pointing angle. The solution to the fin equation has been approximated to determine the temperature distribution along the fin surface for a 5° pointing error.

8. RECOMMENDATIONS

1. An improved analytical model should be developed to describe the performance of the cylindrical focusing parabolic collector on a month-by-month basis. This would require that performance be completely specified by insolation (diffuse and direct), operating temperatures (inlet and outlet), and ambient temperature.

2. The optimization of the design of the receiver for the parabolic collector should be continued.

3. A second flat plate collector operating with a selective coating ($\alpha/\varepsilon \gg 1.0$) should be investigated while operating in conjunction with the two collectors used in this study.

4. Both types of collectors should be compared while operating at temperatures near 250°F.

5. The performance of both units should be compared under rapidly varying cloud conditions.

6. The apparatus should be modified by the addition of thermostats and recording flowmeters to allow experimentation during conditions of broken cloud cover; by the addition of a system for pressurization, to allow operation at temperatures in excess of 250°F; and by the installation of an integral finned tube of copper or aluminum in the cylindrical parabolic collector, to minimize fouling resistance and to improve fin efficiencies.

9. ACKNOWLEDGEMENTS

The authors wish to thank A.P. Fraas and W.M. Culkowski for their invaluable assistance, J.L. Sharp, H.H. Tuck, and C.D. Greene for the use of their equipment, and H.W. Bertini, D.M. Eissenberg, F.A. Gifford, Jr., E. Lumsdaine, and R.L. Reid for their interest.

10. APPENDIX

10.1 Performance Equations

10.1.1 Flat Plate and Parabolic Collector

The development of the performance equations (i.e., those equations quantifying q_A, q_G, q_B, and q_u) was performed for the flat plate collector (8, 9) and are presented. The parabolic performance equations developed by Kaplan, Ozog, and Bühlmann (13) were revised and are also discussed.

By monitoring the flow rate and inlet and outlet temperatures of the working fluid for each quasi-steady state condition, the observed useful heat $(q_u)_{EXPT}$ can be evaluated where:

$$(q_u)_{EXPT} = \bar{\dot{m}}\, C_p\, (T_{out} - T_{in}) \tag{3}$$

or

$$(Q_u)_{EXPT} = (q_u)_{EXPT}\, \Delta t \tag{4}$$

and Δt is the quasi-steady state time duration. This equation holds for both collector types considered in this study.

10.1.2 Flat Plate Collector

The total energy absorbed by the collector plate q_A' is directly proportional to the sum of direct and diffuse incident solar radiation flux incident on the tilted collector surface since the flat plate absorbs both forms of solar radiation. Thus,

$$q_A' = [(H_{TOT} - H_{DIF})A'R_D\tau_e\alpha + H_{DIF}A'R_S(\tau_e\alpha)_S] \tag{5}$$

where $H_{TOT} - H_{DIF}$ is the total solar radiation flux minus the diffuse, i.e., the direct solar radiation flux. $\tau_e\alpha$ is the product of the overall effective direct radition transmittance and the direct radiation absorptivity of the blackened collector plate. R_D is the direct radiation orientation factor which takes into consideration the tilted collector surface from the horizontal. $R_S(\tau_e\alpha)_S$ corresponds to the diffuse radiation components of these effects. R_D can be represented as:

$$R_D = \frac{\cos\theta_T}{\cos\theta_Z} \tag{6}$$

where $\cos\theta_T$ is the direct solar radiation incident on a tilted plate and $\cos\theta_Z$ is the direct solar radiation incident on a plate in the horizontal position.

$$\cos\theta_Z = \sin\Phi\sin\delta + \cos\Phi\cos\delta\cos\omega \tag{7}$$

$$\cos\theta_T = \sin(\Phi - \beta)\sin\delta + \cos(\Phi - \beta)\cos\delta\cos\omega \tag{8}$$

Φ, δ, ω, and β are the latitude, declination of the sun, local hour angle, and tilt angle of the collector plate respectively. The orientation factor R_S for the sky component of the radiation, assuming a uniform intensity-distribution over the sky, is:

$$R_S = \tfrac{1}{2}(1 + \cos\beta) \tag{9}$$

$\tau_e\alpha$ is a function of the angle of solar incidence on the tilted plate, θ_T, and the number of glass plates n. Plots of $\tau_e\alpha$ versus θ_T are available (10). A good approximation of $(\tau_e\alpha)_S$ can be obtained using a value corresponding to an angle of incidence of 58° (10).

The flat plate collector is shown in Fig. 13 to aid in the description of the losses from the plate above to the glass plate(s) and out to the atmosphere (q_G') and the losses from the plate below through the insulation and wood and out to the atmosphere (q_B') (9).

$$q_G' = \frac{A_G'(T_5' - T_o)}{\dfrac{n'}{C\left(\dfrac{T_5' - T_o}{n' + f}\right)^{0.25}} + \dfrac{1}{h_{air}^{\circ}}} + \frac{\sigma A_G'(T_5'^4 - T_o^4)}{\dfrac{1}{\varepsilon_c} + \dfrac{2n' + f + 1}{\varepsilon_G} - n'} \tag{10}$$

where q_G' is the sum of the steady state convective and radiative losses from the collector plate to the atmosphere for n glass plates (9).

$$C = \frac{h_{air}^{i}}{(T_5' - T_o)^{0.25}} \tag{11}$$

Values for C as a function of β are available (9). $h_{air}^{\circ} = 1.0$ Btu/ft^2-hr-°F corresponding to a wind speed of 3 mph was used and a corresponding value of 0.76 for f (9). f is the ratio of the thermal resistance of the outer plate to that of the inner plate. The emissivities of the glass and collector surface are ε_G and ε_C.

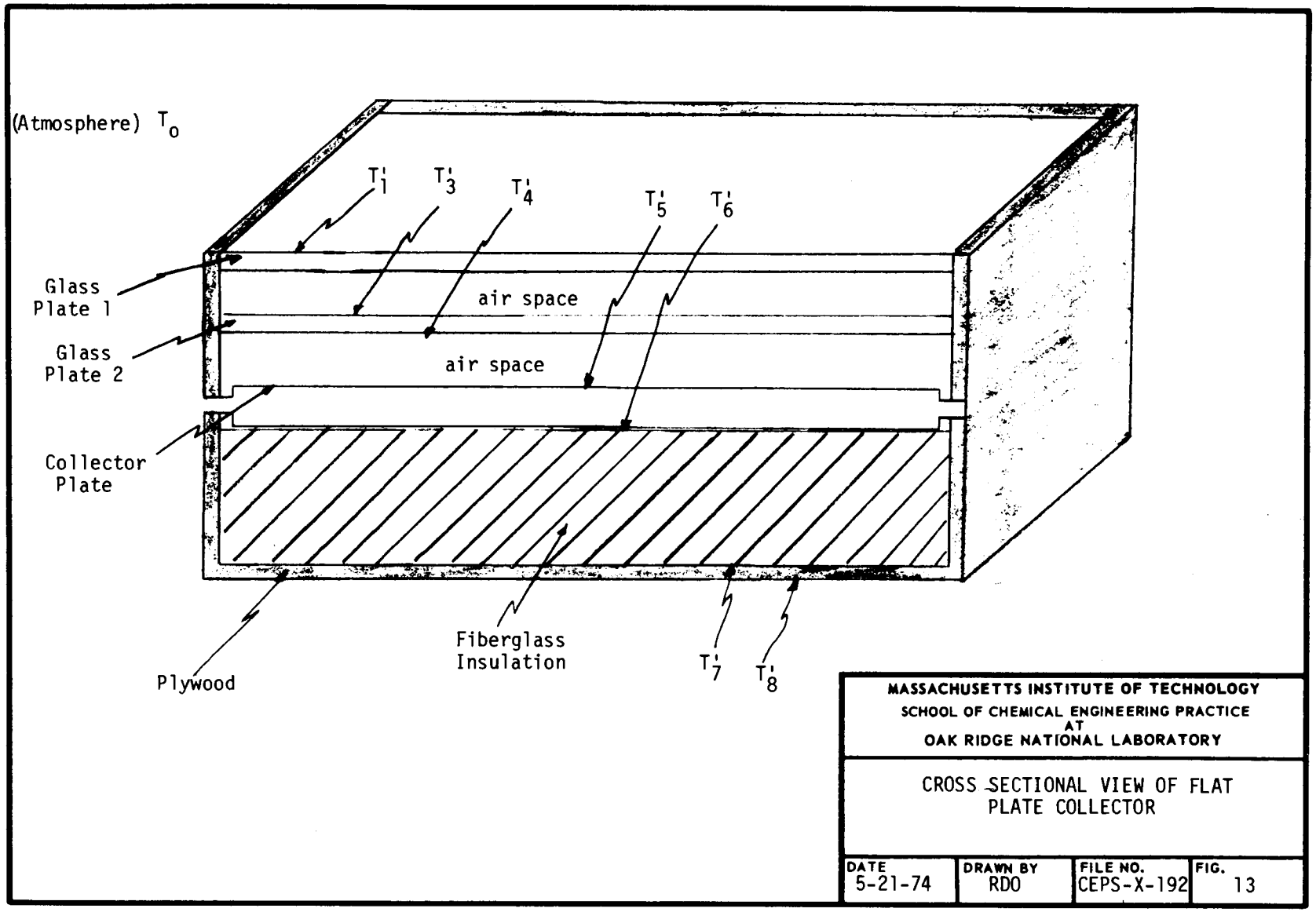
(Atmosphere) T_o
T'_1
T'_3
T'_4
T'_5
T'_6
Glass Plate 1
Glass Plate 2
air space
air space
Collector Plate
Plywood
Fiberglass Insulation
T'_7
T'_8
MASSACHUSETTS INSTITUTE OF TECHNOLOGY
SCHOOL OF CHEMICAL ENGINEERING PRACTICE
AT
OAK RIDGE NATIONAL LABORATORY
CROSS SECTIONAL VIEW OF FLAT PLATE COLLECTOR
DATE 5-21-74
DRAWN BY RDO
FILE NO. CEPS-X-192
FIG. 13

$$q_B' = \frac{T_6' - T_7'}{\frac{X_I'}{k_I A_I'}} = \frac{T_7' - T_8'}{\frac{X_w}{k_w A_w'}} = \frac{T_6' - T_8'}{\frac{X_I'}{k_I A_I'} + \frac{X_w}{k_w A_w'}} = h_{air}^{i} A_I' (T_5' - T_6') \tag{12}$$

$$= \frac{T_5' - T_o}{\frac{1}{h_{air}^{i} A_I'} + \frac{X_I'}{k_I A_I'} + \frac{X_w}{k_w A_w'} + \frac{1}{h_{air}^{o} A_w'}} \tag{13}$$

where q_B' is the sum of the steady state convective and conductive losses. h_{air}^{o} was approximated as 1.0 Btu/ft^2-hr-°F where $h_{air}^{i} = 0.27\ (T_5 - T_6)^{0.25}$ for free convection from horizontal heated plates facing downward at atmospheric pressure for laminar flow (14).

A theoretical useful rate of heat gained by the working fluid may now be evaluated by

$$q_u' = q_A' - (q_B' + q_G') \tag{14}$$

or

$$Q_u' = [q_A' - (q_B' + q_G')]\Delta t \tag{15}$$

10.1.3 Parabolic Focusing Collector

The total energy absorbed is the solar direct radiation flux incident on the projected aperture area plus the direct and diffuse solar radiation flux incident on the glass area minus the projected area of the aperture.

$$q_A = A(H_{TOT} - H_{DIF})R_D\tau_e\Lambda + (A_G - A)(1 - r_{eff})(H_{TOT} - H_{DIF})R_D\tau_e$$

$$+ (A_G - A)(1 - r_{eff})H_{DIF}\, R_S(\tau_e)_S \tag{16}$$

where:

r_{eff} = effective reflectivity of the aluminum foil (top of insulation)

Λ = a shape factor accounting for pointing errors due to misalignment of the parabolic receiver and shading effects

For pointing errors of 4° or less, $\Lambda = 1.0$ assuming a fin efficiency of 100%. r_{eff} has been assumed equal to 0.75 for all heat calculations performed. This term takes into consideration both the reflectivity of the aluminum foil on top of the insulation and the view factor accounting for that radiation which leaves the collector unit after intersecting the outer aluminum surface of the aluminum. Blackening the surface with a high absorptivity paint would eliminate the r_{eff} approximation.

Figure 14 is a sketch of the parabolic focusing collector with all observed temperatures noted. The heat loss through the glass consisting of convective and radiative heat transfer for one glass plate is:

$$q_G = h^o_{air}A_G(T_2 - T_o) + \sigma\varepsilon_G A_G(T_2^4 - T_o^4)$$

$$= h^i_{air}A_G(T_5 - T_2) + h^i_{air}A_R(T_6 - T_2) + \sigma\varepsilon_R A_R(T_6^4 - T_2^4)(1 - \frac{\gamma}{360})$$

$$+ \sigma\varepsilon_R A_R(T_6^4 - T_5^4)(\frac{\gamma r}{360}) \qquad (17)$$

where:

γ = view factor representing that portion of the receiver which the reflector sees.

r = specular reflectivity of the reflector (0.87 for Alzak aluminum)

q_G accounts for steady state convective and radiative heat loss from the glass surface to the atmosphere and the steady state convective losses from the reflector and receiver plus the steady state radiative losses from the receiver to the glass and re-radiation from the receiver to the reflector to the glass. No radiant heat is transmitted through the glass since glass is opaque to the long wavelengths characteristic of source temperature of about 200°F (9).

The heat losses behind the reflector are conductive and convective.

$$q_B = \frac{T_8 - T_9}{\frac{X_w}{k_w A_w}} = \frac{T_5 - T_o}{\frac{1}{h^i_{air}A_I} + \frac{X_I}{k_I A_I} + \frac{X_w}{k_w A_w} + \frac{1}{h^o_{air}A_w}} \qquad (18)$$

The theoretical useful heat gained by the working fluid is analogous to Eq. (13),

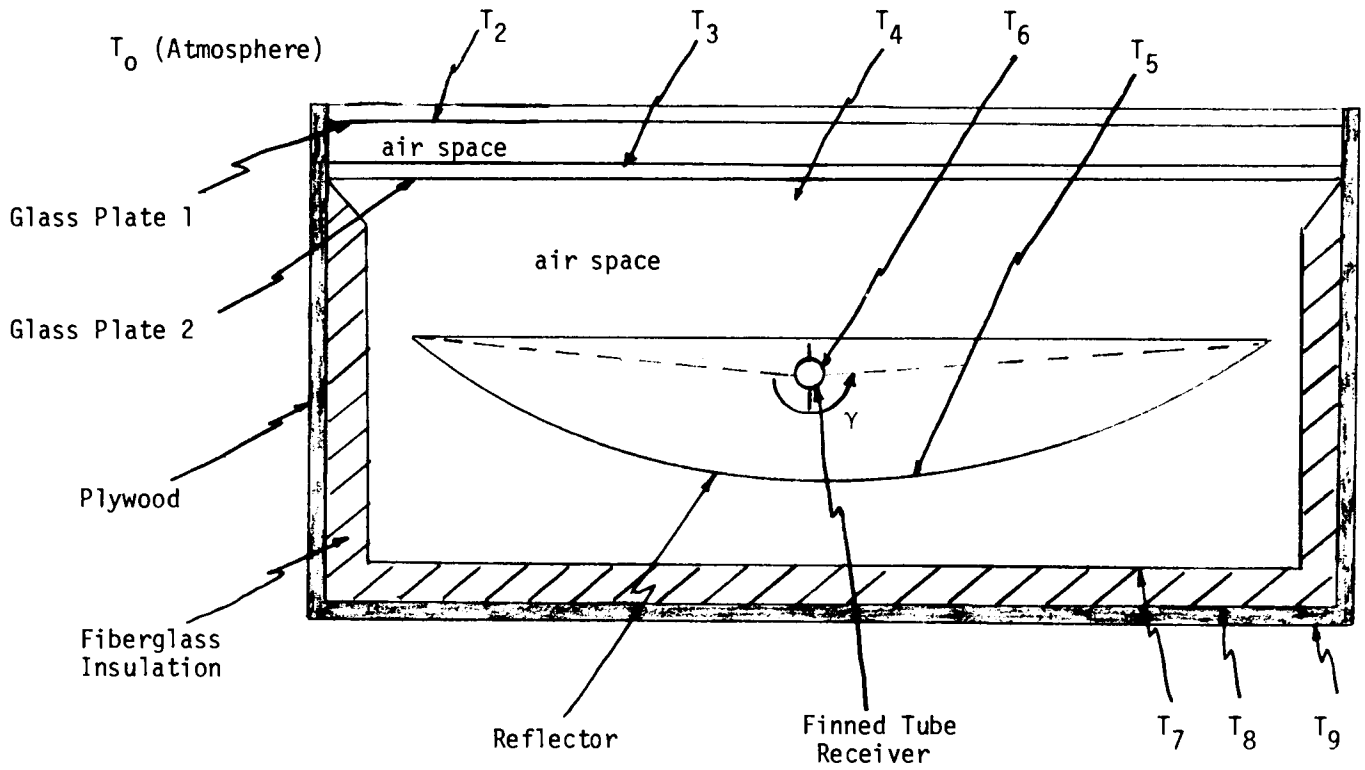

MASSACHUSETTS INSTITUTE OF TECHNOLOGY
SCHOOL OF CHEMICAL ENGINEERING PRACTICE
AT
OAK RIDGE NATIONAL LABORATORY

CROSS SECTION END VIEW OF
PARABOLIC CYLINDRICAL COLLECTOR

DATE	DRAWN BY	FILE NO.	FIG.
5-21-74	RDO	CEPS-X-192	14

$$q_u = q_A - (q_B + q_G) \tag{19}$$

$$Q_u = [q_A - (q_B + q_G)]\Delta t \tag{20}$$

10.2 Sample Calculations

Data obtained from Run 13, performed on 5-14-74 will be used to calculate performance variables for the flat plate collector and the parabolic focusing collector. Quasi-steady state operation was maintained for 32 min (10:23 am to 10:55 am) for both collectors which were tilted 20.5° south toward the celestial equator.

10.2.1 Flat Plate Collector Heat Loss

The total energy absorbed by the blackened collector plate, Q_A', is:

$$Q_A' = A'(H_{TOT} - H_{DIF})\Delta t R_D \tau_e \alpha + A' H_{DIF} \Delta t R_S (\tau_e \alpha)_S \tag{21}$$

where:

A' is the collector plate area = 5.9 ft^2 (see Appendix 10.6)

For a Δt = 32/60 = 0.533 hours of quasi-steady state operation, the radiation fluxes obtained from the total and diffuse pyrheliometer readings were:

$$H_{TOT}\Delta t = 121.5 \text{ Btu/ft}^2$$

$$H_{DIF}\Delta t = 19.2 \text{ Btu/ft}^2$$

To determine R_D, cos θ_Z and cos θ_T must be evaluated [Eqs. (7) and (8)]. The average time during the run was 10:39 am corresponding to 10:39 - 1:36 pm or -177/60 hours east of solar noon. Therefore the hour angle ω is:

$$\omega = -\frac{177}{60} \text{hr}(15°/\text{hr}) = -44.25°$$

In addition, the declination δ, latitude ϕ, and tilt angle β were:

δ = 18.4° corresponding to May 14, 1974

ϕ = 36° (Oak Ridge location)

$$\beta = 20.5°$$

$$\cos\theta_Z = \sin\delta\sin\Phi + \cos\Phi\cos\delta\cos\omega$$

$$= \sin(18.4°)\sin(36°) + \cos(36°)\cos(18.4°)\cos(-44.25°)$$

$$= 0.7354$$

$$\cos\theta_T = \sin\delta\sin(\Phi - \beta) + \cos(\Phi - \beta)\cos\delta\cos\omega$$

$$= \sin(18.4°)\sin(36° - 20.5°) + \cos(36° - 20.5°)\cos(18.4°) \times \cos(-44.25°)$$

$$= 0.7394$$

$$\theta_T = 42.32° \text{ (angle of incidence)}$$

$$R_D = \frac{\cos\theta_T}{\cos\theta_Z} = \frac{0.7394}{0.7354} = 1.005$$

From Fig. 12b of Hottel and Whillier (10), for $\theta_T = 42.32°$, $\tau_e\alpha = 0.72$ and n = 2 glass plates. They suggest that a good approximation to the effective transmittance for the diffuse component of the radiation is a value corresponding to an angle of incidence of 58°.

$$(\tau_e\alpha)_S \text{ for } \theta_T = 58° = 0.60$$

The diffuse radiation orientation factor is a function of the tilt of the box,

$$R_S = \frac{1}{2}(1 + \cos\beta) = \frac{1}{2}[1 + \cos(20.5)] = 0.97 \qquad (22)$$

The total absorbed energy can now be calculated using Eq. (5).

$$Q_A' = 5.9[(121.5 - 19.2)(1.005)(0.72) + (19.2)(0.97)(0.60)]$$

$$= 503 \text{ Btu}$$

In calculating Q_B' the average of the calculated loss through the insulation and through the wood and insulation combined was evaluated.

$$q'_B = \frac{1}{2}\left[\frac{T'_6 - T'_7}{\frac{X'_I}{k_I A'_I}} + \frac{T'_6 - T'_8}{\frac{X'_I}{k_I A'_I} + \frac{X'_w}{k_w A'_w}}\right] \tag{23}$$

and

$$Q'_B = q'_B \, \Delta t \tag{24}$$

See Appendix 10.6 for dimensions and properties and Appendix 10.8 for temperatures.

$$Q'_B = \frac{1}{2}\left[\frac{118 - 72}{\frac{0.42}{(0.023)(10.1)}} + \frac{118 - 69}{\frac{0.42}{(0.023)(10.1)} + \frac{0.0625}{(0.07)(17.1)}}\right]\left(\frac{32}{60}\right)$$

$$= \frac{1}{2}(25.44 + 26.34)\left(\frac{32}{60}\right) = 14 \text{ Btu}$$

For the heat losses through the glass and atmosphere [Eq. (10)],

$$q'_G = \frac{A'_G(T'_5 - T_o)}{\frac{n'}{C\left(\frac{T'_5 - T_o}{n' + f}\right)^{1/4}} + \frac{1}{h^o_{air}}} + \frac{\sigma A'_G(T'^4_5 - T_o^4)}{\frac{1}{\varepsilon_C} + \frac{2n' + f - 1}{\varepsilon_G} - n'} \tag{25}$$

and

$$Q'_G = q'_G \, \Delta t \tag{26}$$

where n' is the number of cover plates and f = 0.76 is the ratio of the thermal resistance of the outer glass plate to that of the inner plate. A value of C = 0.175 was used [see Ref. (9)]. See Appendix 10.6 for dimensions and properties and Appendix 10.8 for temperatures.

$$q'_G = \frac{9.23(125 - 72)}{\frac{2}{0.175\left(\frac{125 - 72}{2 + 0.76}\right)^{1/4}} + \frac{1}{1}} + \frac{0.1723(9.23)\left[\left(\frac{585}{100}\right)^4 - \left(\frac{532}{100}\right)^4\right]}{\frac{1}{0.98} + \frac{2(2) + 0.76 - 1}{0.94} - 2}$$

$$Q'_G = (75.73 + 194.88)\left(\frac{32}{60}\right) = 144 \text{ Btu}$$

The calculated useful heat is

$$Q'_U = Q'_A - (Q'_G + Q'_B) = 503 - (144 + 14) = 345 \text{ Btu} \qquad (27)$$

The experimentally observed useful heat is calculated from the temperature rise of the working fluid.

$$(Q'_U)_{EXPT} = \dot{m}\, C_p (T'_L - T'_o)(\Delta t) \qquad (28)$$

$$= (114 \frac{cc}{min})(\frac{0.991\ g}{cc})(1.0 \frac{cal}{g\text{-}°C})(\frac{°C}{1.8°F})(135° - 84°F)$$

$$(32 \text{ min})(\frac{Btu}{252 \text{ cal}})$$

$$= 406 \text{ Btu}$$

The difference between calculated and experimental values is

$$\left[\frac{(Q'_U)_{EXPT} - (Q'_U)}{(Q'_U)_{EXPT}}\right](100) = (\frac{406 - 345}{406})(100) = (\frac{61}{406})(100) = 15\%$$

10.2.2 Parabolic Focusing Collector Heat Losses

The total energy absorbed by the collector is

$$Q_A = A(H_{TOT} - H_{DIF})\Delta t\, R_D\, \tau_e \Lambda\alpha + (A_G - A)(1 - r_{eff})(H_{TOT} - H_{DIF})\Delta t R_D \tau_e$$

$$+ (A_G - A)(1 - r_{eff}) H_{DIF}\, \Delta t R_S (\tau_e)_S \qquad (16)$$

where a shape factor $\Lambda = 1.0$ was assumed for the focused collector (all radiation reflected by the reflector strikes the receiver). The effective transmittance can be calculated from the values of $\tau_e\alpha$ and $(\tau_e\alpha)_S$ assuming $\alpha_S \cong 0.90$ and $\alpha = 0.98$ from Hottel and Whillier's graph (10).

$$\tau_e = 0.735 \text{ for } \theta_T = 42.32°$$

$$\tau_e)_S = 0.67 \text{ for } \theta_T = 58°.$$

Upon substitution (see Appendices 10.2.1 and 10.6) for Run 13 with α for the receiver surface = 0.87,

$$Q_A = 11.57(121.5 - 19.2)(1.005)(0.735)(1.0)(0.87)$$
$$+ (15.68 - 11.57)(1 - 0.75)(121.5 - 19.2)(1.005)(0.735)$$
$$+ (15.68 - 11.57)(1 - 0.75)(19.2)(0.97)(0.67)$$
$$= 851 \text{ Btu}$$

The average of the heat loss through the wood and the heat loss based on an overall coefficient was used to estimate Q_B.

$$q_B = \frac{1}{2}\left[\frac{T_8 - T_9}{\frac{X_w}{k_w A_w}} + \frac{T_5 - T_o}{\frac{1}{h^i_{air} A_I} + \frac{X_I}{k_I A_I} + \frac{X_w}{k_w A_w} + \frac{1}{h^o_{air} A_w}}\right] \tag{29}$$

and

$$Q_B = q_B \, \Delta t \tag{30}$$

See Appendix 10.6 for physical properties and Appendix 10.8 for temperatures.

$$Q_B = \frac{32}{60}\left(\frac{1}{2}\right)\left[\frac{81 - 70}{\frac{0.0625}{(0.07)(42.88)}} + \frac{116 - 72}{\frac{1}{1(37.31)} + \frac{0.104}{(.023)(37.31)} + \frac{0.0625}{(.07)(42.88)} + \frac{1}{1(42.88)}}\right]$$
$$= 202 \text{ Btu}$$

Q_G is similarly calculated by averaging the losses from the glass surface to the atmosphere with the losses from the reflector and receiver to the glass plate.

$$q_G = \frac{1}{2}\left[\{h^o_{air} A_G (T_2 - T_o) + \sigma\varepsilon_G A_G (T_2^4 - T_o^4)\} + \{h^i_{air} A_G (T_5 - T_2)\right.$$
$$+ h^i_{air} A_R (T_6 - T_2) + \sigma\varepsilon_R A_R (T_6^4 - T_2^4)(1 - \frac{\gamma}{360})$$
$$\left. + \sigma\varepsilon_R A_R (T_6^4 - T_5^4)(\gamma r/360)\}\right] \tag{31}$$

and

$$Q_G = q_G \, \Delta t \tag{32}$$

$$Q_G = (\frac{32}{60})(\frac{1}{2}) \{(1)(15.68)(98 - 72) + 0.1723(0.94)(15.68)[(\frac{558}{100})^4 - (\frac{532}{100})^4]\}$$

$$+ \{(0.235)(15.68)(116 - 98) + 0.235(2.76)(183 - 98)$$

$$+ 0.1723(0.87)(2.76)(1 - \frac{197}{360})[(\frac{643}{100})^4 - (\frac{558}{100})^4]$$

$$+ 0.1723(0.87)(2.76)(\frac{197(0.87)}{360})[(\frac{643}{100})^4 - (\frac{576}{100})^4]\}$$

$$= (\frac{32}{60})(\frac{1}{2})[\{408 + 428\} + \{66 + 55 + 139 + 120\}]$$

$$= 324 \text{ Btu}$$

The theoretical useful heat gained by the working fluid is:

$$Q_u = Q_A - (Q_B + Q_G) \tag{33}$$

$$= 851 - (202 + 324) = 325 \text{ Btu}$$

The experimentally observed useful heat is

$$(Q_u)_{EXPT} = \dot{m}\, C_p(T_{out} - T_{in})\Delta t$$

$$= (105)(0.991)(1.00)(138 - 84)(32)(\frac{1}{1.8(252)})$$

$$= 396 \text{ Btu}$$

The difference between calculated and experimental values is:

$$\frac{(Q_u)_{EXPT} - Q_u}{(Q_u)_{EXPT}}(100) = \frac{396 - 325}{396}(100) = 18\%$$

10.3 Theoretical Development of Efficiencies Based on Monthly Averages

10.3.1 Calculation of Weather Parameters

To estimate the efficiencies (eff) of both the flat plate and the parabolic collectors, as monthly averages throughout the year, the total direct and diffuse radiation incident on the collectors had to be determined. The total radiation incident on a horizontal surface (pyrheliometer) was available from a computer output compiled by Culkowski (4). This consisted of daily averages of total radiation for each day of the year for a period of 16 years.

A monthly average was determined and is tabulated in Table 5. The average for each month for the 16 years was then calculated and was used in calculating the efficiencies of both units.

The direct and diffuse radiations were not available and had to be calculated from the total radiation, the sky cover, and the turbidity (B). The sky cover (Y) was available as the monthly average for every year for Oak Ridge (5). The average values of turbidity (B) used for each month beginning with January were 0.06, 0.08, 0.10, 0.13, 0.15, 0.22, 0.37, 0.39, 0.28, 0.19, 0.10, and 0.05.

The following assumptions were made in calculating the direct and diffuse components:

1. The diffuse radiation was calculated as diffuse radiation with clouds present (H_{DIF_1}) and as diffuse radiation when there were no clouds (H_{DIF_2}) (sky cover = 0)

2. The average penetration of diffuse radiation (V) through a cloud was assumed to be 50% at all times.

Therefore the diffuse radiation with cloud cover would be (3):

$$H_{DIF_1} = \overline{H}_{TOT} \cdot Y \cdot V \tag{34}$$

The difference of the total radiation and the diffuse radiation with cloud cover is equal to the sum of the direct radiation and diffuse radiation without cloud cover.

$$\overline{H}_{TOT} - H_{DIF_1} = H_{D_1} + H_{DIF_2} \tag{35}$$

Direct radiation was calculated by including the turbidity factor B as:

$$H_{D_1} = (\overline{H}_{TOT} - H_{DIF_1})10^{-B} \tag{36}$$

Table 5. Calculation of Average Value of Total Radiation for 1956-1971 on Monthly Basis (cal/cm^2-day)

Year	Jan.	Feb.	March	April	May	June	July	Aug.	Sept.	Oct.	Nov.	Dec.
1956	168.65	221.50	418.84	517.57	546.10	584.80	537.55	565.29	470.33	320.58	214.47	164.06
1957	144.58	226.54	308.48	495.50	568.52	474.23	596.94	534.87	327.60	270.35	209.37	151.06
1958	185.13	311.79	255.55	376.50	502.06	587.43	452.23	480.55	435.80	342.26	232.43	189.74
1959	206.58	252.68	359.19	424.70	483.39	552.47	498.74	478.23	387.10	291.03	226.13	151.00
1960	164.13	244.24	328.13	473.20	532.19	521.20	533.42	415.06	377.77	268.65	221.10	186.71
1961	219.13	217.00	268.23	399.40	453.61	451.10	449.42	425.39	412.57	302.65	181.87	137.16
1962	168.39	230.39	286.71	423.57	552.06	519.93	519.26	512.32	386.73	309.39	184.27	171.00
1963	192.74	269.82	369.29	436.50	510.39	462.83	458.61	453.71	407.00	369.00	190.37	170.71
1964	212.87	226.39	322.23	386.87	524.29	565.43	461.48	457.23	413.40	326.35	223.87	140.23
1965	185.45	250.64	290.61	415.97	513.00	474.60	433.60	437.96	339.17	298.58	177.30	161.81
1966	153.42	212.39	405.10	428.00	531.84	594.77	518.13	454.52	341.83	349.97	174.67	150.84
1967	205.32	265.11	411.90	500.87	441.13	528.07	421.39	423.32	408.37	352.58	244.83	155.74
1968	182.68	316.10	381.58	420.87	499.77	558.40	520.48	511.19	389.73	299.42	203.40	170.94
1969	180.65	248.93	368.29	452.14	533.29	525.37	532.39	482.26	394.13	306.48	231.63	143.29
1970	186.10	240.61	315.71	410.23	545.35	500.27	514.65	417.58	372.57	289.94	197.33	156.87
1971	165.16	249.79	341.13	482.10	496.94	504.17	411.35	456.94	349.87	294.23	218.03	121.77
$\sum$	2920.98	3983.92	5430.97	7043.99	8233.93	8405.07	7859.64	7506.42	6213.97	4991.46	3331.07	2522.93
Avg. $\overline{H}_{TOT}$	182.56	249.00	339.44	440.25	514.62	525.32	491.23	469.15	388.37	311.97	208.19	157.68

The diffuse radiation with no clouds was calculated from Eq. (37). The total diffuse radiation $H_{DIF,TOT}$ was calculated as:

$$H_{DIF,TOT} = H_{DIF_1} + H_{DIF_2} \tag{37}$$

The average values of direct and total diffuse radiation for each month for the period of 16 years were then calculated and tabulated in Tables 6 and 7. The average values for each month over the entire period were used to calculate the total absorbed energy by the collectors.

Sample Calculation for Jan. 1971:

From Table 5, $\overline{H}_{TOT}$ = 165.16 cal/cm^2-day. Sky cover Y = 0.54. Therefore, from Eq. (34) we can calculate

$$H_{DIF_1} = (165.16)(0.54)(0.5) = 44 \text{ cal/cm}^2\text{-day}$$

From Eq. (36),

$$H_{D_1} = (165.16 - 44.59)\ 10^{-0.06} = 105 \text{ cal/cm}^2\text{-day}$$

From Eq. (35),

$$H_{DIF_2} = 165 - 44 - 105 = 16 \text{ cal/cm}^2\text{-day}$$

From Eq. (37),

$$H_{DIF,TOT} = 44 + 16 = 60 \text{ cal/cm}^2\text{-day}$$

10.3.2 Calculation of Theoretical Efficiencies of the Flat Plate Collector

The efficiency of the flat plate was calculated theoretically as the ratio of useful radiation (q_u'/A') to total radiation incident on the collector. The useful energy was calculated as:

$$\frac{q_u'}{A'} = \frac{q_A'}{A'} - \frac{q_B'}{A'} - \frac{q_G'}{A'} \tag{38}$$

and the total radiation was calculated from the direct and diffuse radiation corrected for the tilt of the collector as

Table 6. Calculation of Average Value of Direct Radiation for 1956-1971 on a Monthly Basis (cal/cm^2-day)

Year	Jan.	Feb.	March	April	May	June	July	Aug.	Sept.	Oct.	Nov.	Dec.
1956	94.01	113.30	229.00	258.32	270.63	255.47	153.64	169.26	190.06	149.03	121.81	104.55
1957	75.55	118.71	158.05	262.63	281.74	191.45	194.80	183.03	107.45	113.46	111.65	90.20
1958	107.11	199.26	120.12	188.06	245.96	267.87	129.32	149.74	172.23	174.64	133.12	123.27
1959	122.21	134.22	127.26	216.85	245.39	248.61	144.76	142.15	135.87	128.64	125.05	84.67
1960	90.67	129.74	164.61	262.63	285.28	217.34	166.29	120.82	144.38	125.73	131.01	149.42
1961	142.06	120.67	128.20	198.02	222.22	178.64	128.51	123.83	173.77	160.33	94.83	76.30
1962	93.03	130.03	141.56	228.81	317.49	227.73	173.33	172.24	207.08	158.87	93.89	106.53
1963	120.73	157.89	205.68	229.34	269.97	181.89	138.04	140.45	167.20	221.86	103.77	122.33
1964	137.05	131.53	176.92	188.95	273.60	256.14	155.77	134.97	165.53	171.82	131.76	79.25
1965	111.33	143.54	148.08	220.09	274.99	202.18	131.45	129.29	128.75	154.29	98.05	97.21
1966	84.76	107.53	233.62	186.86	258.86	276.57	152.62	121.13	120.87	178.57	86.93	85.25
1967	118.79	145.23	234.29	263.16	203.58	215.45	107.81	108.48	146.52	171.88	140.23	83.86
1968	104.10	186.28	211.01	208.67	232.42	231.18	147.77	155.10	135.78	136.24	99.03	96.61
1969	98.23	137.40	196.39	173.83	287.76	215.93	165.97	143.35	139.36	143.43	129.01	80.34
1970	111.72	131.80	159.38	188.21	300.08	207.11	164.87	114.71	131.74	128.15	174.49	88.66
1971	104.89	135.80	185.95	274.70	250.51	207.21	105.24	126.46	116.44	131.01	121.43	65.57
$\sum$	1716.24	2222.93	2820.12	3558.13	4220.48	3580.77	2360.19	2235.01	2383.03	2447.95	1896.66	1534.02
Avg. $\overline{H}_{D_1}$	107.27	138.93	176.26	222.38	263.78	223.80	147.51	139.69	148.94	153.00	118.54	95.88

Table 7. Calculation of Average Value of Diffuse Radiation for 1956-1971 on Monthly Basis (cal/cm^2-day)

Year	Jan.	Feb.	March	April	May	June	July	Aug.	Sept.	Oct.	Nov.	Dec.
1956	74.64	108.20	189.28	259.25	275.47	329.33	383.91	395.13	280.27	171.55	92.66	59.51
1957	69.02	107.83	150.43	232.87	286.79	282.78	402.14	351.84	220.15	156.89	97.72	60.86
1958	78.02	112.53	135.43	188.44	256.10	319.56	322.91	330.81	263.57	167.62	99.31	66.47
1959	84.37	118.46	125.42	207.85	238.00	303.86	353.98	336.08	251.23	162.39	101.08	66.33
1960	73.46	114.50	163.52	210.57	246.91	303.86	367.13	294.24	233.39	142.92	90.10	71.68
1961	77.07	96.33	140.03	201.38	231.39	272.46	320.91	301.56	238.80	142.32	87.04	60.86
1962	75.36	100.36	145.15	194.76	234.57	297.20	346.60	340.08	305.24	150.52	90.38	64.47
1963	72.01	111.93	163.61	207.16	240.42	280.94	320.57	313.26	239.80	147.14	86.60	68.04
1964	75.82	94.86	145.31	197.92	250.69	309.29	305.71	322.26	247.87	154.53	92.11	60.98
1965	74.12	107.10	142.53	195.88	238.01	272.42	302.15	308.67	210.42	144.29	79.25	64.60
1966	68.66	104.86	171.48	241.14	273.18	318.21	365.51	333.39	220.96	171.40	87.74	65.59
1967	86.53	119.88	177.61	237.71	273.55	312.62	313.58	314.84	361.85	180.70	104.60	71.88
1968	78.58	129.82	170.57	212.20	267.35	327.22	372.91	356.09	253.95	163.18	103.77	74.33
1969	82.42	111.53	171.90	194.46	245.53	309.44	366.42	338.91	254.77	163.05	102.62	62.95
1970	74.38	108.81	157.33	222.02	245.27	293.15	349.78	302.87	240.83	161.79	115.45	68.21
1971	60.27	113.99	155.18	207.40	246.43	296.96	306.11	330.48	233.43	163.22	96.60	56.20
$\sum$	1204.73	1760.99	2504.78	3411.01	4049.66	4829.30	5500.32	5270.51	4056.53	2544.11	1527.03	1042.96
Avg. $\bar{H}_{DIF,TOT}$	75.30	110.06	156.55	213.19	253.10	301.83	343.77	329.41	253.53	159.01	95.44	65.19

$$H_T = H_{D1}R_D + H_{DIF,TOT}R_S \tag{39}$$

Total energy absorbed, q'_A, heat losses through the box, q'_B, and heat losses through the glass, q'_G, can be calculated using the following equations:

$$\frac{q'_A}{A'} = H_{D1}R_D\tau_e\alpha + H_{DIF,TOT}R_S(\tau_e\alpha)_S \tag{40}$$

$$\frac{q'_B}{A'} = \frac{T_{LM} - T_o}{\frac{X'_I}{k_I}\frac{A'}{A'_I} + \frac{X'_w}{k_w}\frac{A'}{A'_w} + \frac{1}{h^o_{air}}\frac{A'}{A'_w} + \frac{1}{h^i_{air}}\frac{A'}{A'_I}} \tag{41}$$

$$\frac{q'_G}{A'_G} = \frac{T_{LM} - T_o}{\frac{n'}{C\left(\frac{T - T_o}{n' + f}\right)^{1/4}} + \frac{1}{h^o_{air}}} + \frac{\sigma(T^4_{LM} - T^4_o)}{\frac{1}{\varepsilon_c} + \frac{2n' + f + 1}{\varepsilon_G} - n'} \tag{42}$$

Efficiencies were calculated for three different operating conditions. The inlet temperature of the working fluid (in this case water) was assumed constant at 100°F and the outlet was set at 135, 165, and 185°F, respectively. Varying the tilt of the reflector will cause the efficiencies of the flat plate to change as the direct and diffuse terms are dependent on the orientation factors (R_D and R_S). Two cases were studied using tilt angles β equal to the latitude (ϕ) and the latitude + 15°. The latter case favors the winter solstice (9). Finally a third case was considered which calculated maximum efficiencies using maximum total radiation for each month assuming zero sky cover and tilt angle equalling the latitude. For all three cases these assumptions were made:

1. Efficiencies were calculated for conditions at solar noon.

2. Two window glass plates not surface treated with half inch spacing between them were used.

3. Declination of the sun δ was taken as the average of each month from values in Smithsonian Meteorological tables (1).

4. The temperature of the flat plate (T_{LM}) was calculated as the log mean temperature of the inlet and outlet water temperature.

5. Average ambient temperature for each month was used to calculate heat losses.

Results for all three cases are tabulated in Tables 8, 9, and 10. Table 8 is a tabulation of the total, direct, and diffuse radiation incident on the collector; Table 9 is a tabulation of the ambient temperatures and heat losses for the three different operating temperatures (identical for all three cases); Table 10 is a tabulation of the efficiencies for the three cases and three different operating temperatures.

A sample calculation for January Case 1 with an operating temperature (T_{out}) of 135°F is:

$$\beta = \phi$$

$$\omega = 0 \qquad \cos\omega = 1.0$$

$$\phi = 36° \qquad \cos\phi = 0.81 \qquad \sin\phi = 0.59$$

$$\delta = -20.36° \qquad \cos\delta = 0.94 \qquad \sin\delta = -0.35$$

$$R_S = \frac{1}{2}(1 + \cos\phi) = \frac{1}{2}(1 + 0.81) = 0.905$$

$$R_D = \frac{\cos\theta_T}{\cos\theta_Z}$$

where:

$$\cos\theta_T = \sin(\phi - \beta)\sin\delta + \cos(\phi - \beta)\cos\delta\cos\omega$$

$$= 0 + \cos\delta = 0.94$$

$$\cos\theta_Z = \sin\phi\sin\delta + \cos\phi\cos\delta\cos\omega$$

$$= (0.59)(-0.35) + (0.81)(0.94)(1) = 0.55$$

$$R = \frac{0.94}{0.55} = 1.709$$

$\tau_e\alpha$ was obtained from Fig. 12b from Hottel and Woertz (9) for a θ_T of 20.63° and two glass plates (untreated window glass). $\tau_e\alpha = 0.775$. $(\tau_e\alpha)_S$ from the same figure for a θ_T of 58° and two glass plates was 0.6. Using the average radiation fluxes for January (see Fig. 10),

$$\frac{q_A}{A'} = H_{D_1}R_D\tau_e\alpha + H_{DIF,TOT}R_S(\tau_e\alpha)_S$$

$$= (41.665)(1.709)(0.775) + (29.25)(0.905)(0.6) = 71.07 \text{ Btu/hr-ft}^2 \text{ of aperture}$$

Table 8. Solar Energy Flux Incident on Flat Plate

	Total Radiation (cal/cm^2-day)			Direct Radiation (cal/cm^2-day)			Diffuse Radiation (cal/cm^2-day		
	Case 1	Case 2	Case 3	Case 1	Case 2	Case 3	Case 1	Case 2	Case 3
Jan.	97.68	99.4	213.14	71.21	75.6	197.51	26.47	23.8	15.63
Feb.	107.16	105.8	219.01	72.16	74.3	194.60	35.00	31.5	24.41
Mar.	117.23	110.9	221.75	71.77	70.0	186.41	45.46	40.8	35.34
Apr.	129.95	118.7	212.60	73.00	67.5	165.33	56.96	51.2	47.28
May	134.56	119.6	192.13	71.96	63.3	140.20	62.61	56.3	51.93
June	127.60	113.0	178.05	55.60	65.0	108.85	72.00	48.0	69.20
July	121.43	110.3	168.96	36.41	33.9	72.56	85.02	76.4	96.40
Aug.	126.21	113.6	172.37	41.59	37.6	76.90	84.62	76.0	95.47
Sept.	119.97	110.6	172.17	52.23	49.7	101.09	67.73	60.9	71.08
Oct.	118.33	113.4	188.83	70.06	70.0	139.13	48.27	43.4	49.68
Nov.	97.22	97.5	183.19	66.86	70.2	159.31	30.35	27.3	23.88
Dec.	84.50	87.1	179.18	62.73	67.5	168.55	21.77	19.6	10.63

Case 1: $\beta = \phi$) average insolation

Case 2: $\beta = \phi + 15°$)

Case 3: $\beta = \phi$ monthly maximum insolation

Table 9. Heat Losses Through the Box and Glass of a Flat Plate*

	Heat Losses Through Bottom of the Box (°F)			Heat Losses Through Glass Plates (°F)			Ambient Temp.
	T_{out}=135	T_{out}=165	T_{out}=185	T_{out}=135	T_{out}=165	T_{out}=185	T_o
Jan.	6.51	7.60	8.31	60.73	73.77	82.46	40.0
Feb.	6.17	7.28	7.99	57.93	70.93	79.60	43.8
Mar.	5.91	7.02	7.73	55.64	68.60	77.25	46.9
Apr.	5.87	6.98	7.69	55.34	68.30	76.95	47.3
May	4.26	5.37	6.08	40.87	53.61	62.13	66.3
June	4.12	5.23	5.94	39.52	52.23	60.75	68.0
July	3.54	4.65	5.36	34.13	46.74	55.21	74.9
Aug.	3.59	4.71	5.41	34.66	47.29	55.75	74.2
Sept.	4.05	5.16	5.87	38.88	51.59	60.10	68.8
Oct.	4.90	6.01	6.72	46.65	59.48	68.06	58.8
Nov.	6.11	7.28	7.99	57.93	70.93	79.60	43.8
Dec.	6.57	7.69	8.39	61.46	74.50	83.20	39.0

*Heat losses through the box and glass of a flat plate are the same for all three cases.

Table 10. Efficiencies of the Flat Plate Collector (%)

	Case 1: $\beta=\phi$ Average Insolation			Case 2: $\beta=\phi+15°$ Average Insolation			Case 3: $\beta=\phi$ Maximum Insolation		
	$T_{out}=135°F$	$T_{out}=165°F$	$T_{out}=185°F$	$T_{out}=135°F$	$T_{out}=165°F$	$T_{out}=185°F$	$T_{out}=135°F$	$T_{out}=165°F$	$T_{out}=185°F$
Jan.	4.0	(-10.5)	(-20.1)	6.0	(-8.2)	(-17.6)	44.7	38.0	33.6
Feb.	12.0	(-1.1)	(-9.1)	12.1	(-1.3)	(-10.2)	46.3	39.8	35.6
March	17.2	6.2	(-1.8)	15.8	3.1	(-5.3)	47.0	40.6	36.4
April	22.8	12.0	4.8	18.1	6.3	(-1.6)	44.8	38.2	33.8
May	34.0	23.7	16.8	30.7	19.2	11.4	49.3	42.1	37.3
June	33.7	22.9	15.7	29.4	17.2	9.0	46.2	38.4	33.2
July	34.3	23.0	15.4	30.8	18.3	10.0	45.2	37.1	31.7
August	31.9	21.0	13.7	32.0	19.9	11.8	44.0	36.0	30.7
Sept.	31.9	20.4	12.7	29.3	16.8	8.4	45.4	37.4	32.0
Oct.	26.9	15.1	7.2	25.7	13.4	5.2	45.6	38.2	33.3
Nov.	6.2	(-8.3)	(-18.0)	7.2	(-7.3)	(-16.9)	40.2	32.5	27.4
Dec.	(-7.4)	(-24.2)	(-35.3)	(-4.2)	(-20.4)	(-31.2)	38.5	30.6	25.3

$$\frac{q_B}{A'} = \frac{T_{LM} - T_o}{\frac{X_I'}{k_I}\frac{A'}{A_I'} + \frac{X_w}{k_w}\frac{A'}{A_w'} + \frac{1}{h^o_{air}}\frac{A'}{A_w'} + \frac{1}{h^i_{air}}\frac{A'}{A_I'}} \tag{41}$$

$T_o = 40°F$

$$T_{LM} = \frac{T_{out} - T_{in}}{\ln(T_{out}/T_{in})} = \frac{135 - 100}{\ln(\frac{135}{100})} = \frac{35}{0.30} = 116.67°F$$

From Appendix 10.6,

$A' = 5.9\ ft^2$

$A_I = 10.1\ ft^2$

$A_w = 17.7\ ft^2$

$X_I = 0.417\ ft$

$X_w = 0.0625\ ft$

$h^i_{air} = h^o_{air} = 1\ Btu/hr\text{-}ft^2\text{-}°F$

$k_w = 0.069\ Btu/hr\text{-}ft\text{-}°F$

$k_I = 0.023\ Btu/hr\text{-}ft\text{-}°F$

$$\frac{q_B'}{A'} = \frac{116.67 - 40}{\frac{0.417}{0.023}(\frac{5.9}{10.1}) + \frac{0.0625}{0.069}(\frac{5.9}{17.7}) + \frac{5.9}{17.7} + \frac{5.9}{10.1}} = 6.5\ Btu/hr\text{-}ft^2 \text{ of aperture}$$

$$\frac{q_G'}{A_G'} = \frac{T_{LM} - T_o}{\frac{n'}{C(\frac{T - T_o}{n' + f})^{\frac{1}{4}}} + \frac{1}{h^o_{air}}} + \frac{\sigma(T_{LM}^4 - T_o^4)}{\frac{1}{\varepsilon_c} + \frac{2n' + f - 1}{\varepsilon_G} - n'} \tag{42}$$

$n = 2$

$C = 0.16$ (9)

$f = 0.76$ (9)

$\varepsilon_c = 0.94$

$\varepsilon_G = 0.98$

$\sigma = 0.1723 \times 10^{-8}\ Btu/hr\text{-}ft^2\text{-}R^4$

$T_{LM}^4 = (116.67 + 460)^4 = 1.106 \times 10^{11}\ °R^4$

$T_o = (40 + 460)^4 = 6.249 \times 10^{10}\ °R^4$

$$\frac{q_G'}{A'} = \frac{q_G'}{A_G'}\left(\frac{A_G'}{A'}\right) = \frac{q_G'}{A_G'}(1.56) = \frac{\dfrac{1.56(116.67 - 40)}{2}}{0.16\left(\dfrac{116.67 - 40}{2 + 0.76}\right)^{1/4} + \dfrac{1}{T}} + \frac{0.2689 \times 10^{-8}(T^4 - T_o^4)}{\dfrac{1}{0.94} + \dfrac{4 + .76 - 1}{0.98} - 2}$$

$$= 60.73 \text{ Btu/hr-ft}^2 \text{ of aperture}$$

Therefore from Eq. (38),

$$\frac{q_u'}{A'} = 71.1 - 60.73 - 6.5 = 3.87 \text{ Btu/hr-ft}^2 \text{ of aperture}$$

and the efficiency is:

$$\text{eff} = \frac{q_u'/A'}{H_T} = \frac{3.87}{97.7}(100\%) = 4\%$$

10.4 Development of Temperature Distribution Along Finned Tube

10.4.1 Steady State Fin Equation

The steady state fin equation for the conditions of the straight fin of uniform thickness [where the modes of heat transfer are conduction, convection, re-radiation, and an unknown radiational energy density, F(y), upon one side of the fin] is given by:

$$\frac{d^2T}{dy^2} - \frac{2h_cL_t}{kA_f}(T - T_\infty) - \frac{2\sigma\varepsilon L_t}{kA_f}(T^4 - T_\infty^4) + \frac{L_tF(y)}{kA_f} = 0 \qquad (43)$$

Defining an effective heat transfer coefficient including radiation, h_{eff}, Eq. (43) becomes:

$$\frac{d^2T}{dy^2} - \frac{2h_{eff}L_t}{kA_f}(T - T_\infty) + \frac{L_tF(y)}{kA_f} = 0 \qquad (44)$$

with boundary conditions:

$$y = 0 \qquad T = t_{wall} \qquad (44.1)$$

$$y = \pm\ell \qquad dT/dy = 0 \tag{44.2}$$

The solution of Eq. (44) yields the unknown useful heat flux to the tube:

$$q_u = -kA_f \left.\frac{dT}{dy}\right|_{y=0} \tag{2}$$

The solution to the fin equation [Eq. (2)] requires the knowledge of the energy distribution along the fin. To define this distributed energy input to the tube, F(y) must be determined for any given pointing angle as a function of the incident radiation to the collector times a geometrical concentration factor , CX, evaluated at each discrete value of y along the finned tube (see Appendix 10.4.2 for further details).

10.4.2 Development of the Energy Distribution Function

The equation for a parabola with focus (0,P) and directrix y=-P is given by:

$$X^2 = 4Py \tag{45}$$

where the slope of the tangent to the parabola is:

$$\frac{dy}{dX} = \frac{X}{2P} \tag{46}$$

If the pointing angle error Ψ is defined as positive if the total angle is greater than 90°, the slope of the reflected ray can be expressed as (see Fig. 4),

$$\frac{dR}{dX} = \cot(2a + \Psi) \tag{47}$$

where a is the angle between the tangent to the reflector and a line drawn normal to the aperture passing through the tangent point, or

$$\frac{dR}{dX} = \frac{\cot\Psi\left(\frac{\cot^2 a - 1}{2\cot a}\right) - 1}{\cot\Psi + \left(\frac{\cot^2 a - 1}{2\cot a}\right)} \tag{48}$$

If it is noted that

$$\cot a = \frac{dy}{dX} \tag{49}$$

and substituting from Eq. (46),

$$\cot a = \frac{X}{2P} \tag{50}$$

then Eq. (48) becomes,

$$\frac{dR}{dX} = \frac{\cot \Psi[\frac{(X^2/4P^2) - 1}{X/P}] - 1}{\cot \Psi + [\frac{(X^2/4P^2) - 1}{X/P}]} \tag{51}$$

Simplifying and using the generalized equation for a line, $y = mx + b$, where $m = dR/dX$, the general equation for a reflected ray from a parabolic mirror with a pointing error is given as:

$$y = X\left[\frac{\cot \Psi(\frac{X}{4P} - \frac{P}{X}) - 1}{\cot \Psi + (\frac{X}{4P} - \frac{P}{X})}\right] + b \tag{52}$$

or for the particular geometric configuration used in this study:

$$b = 0.0644X^2 - \left[\frac{11.43(\frac{X}{15.53} - \frac{3.88}{X}) - 1}{11.43 + (\frac{X}{15.53} - \frac{3.88}{X})}\right] X \quad \text{(all units in inches)} \tag{53}$$

The concentration factor, CX, using one unit of energy normalized over the parabolic aperture can therefore be determined between any two y intercepts (or corresponding Δy) along the finned tube (see program listing and computer output for Solar.F4 in Appendix 10.4.4).

10.4.3 Temperature Distribution Along the Finned Tube

The temperature distribution along the fin can be approximated using Euler's method (given discrete values of $CX|_y$) by the following:

$$\left.\frac{dT}{dy}\right|_{y+\Delta y} = \left.\frac{dT}{dy}\right|_y + H \left.\frac{d^2T}{dy^2}\right|_y \tag{54}$$

$$T|_{y-\Delta y} = T|_y - H \left.\frac{dT}{dy}\right|_y \tag{55}$$

where the boundary conditions are given in Eqs. (44.1) and (44.2) and $H = \Delta y$. The method assumes an initial value for t_{wall} and involves a trial and error solution based on an estimated distribution function. Convergence is routinely obtained as computed $T|_{y-\Delta y}$ approaches the estimated value of $T|_{y-\Delta y}$. Specifically, $dT/dy|_{y+\Delta y}$ is given as:

$$\left.\frac{dT}{dy}\right|_{y+\Delta y} = \left.\frac{dT}{dy}\right|_y + H\left[\frac{2h_{eff}L_t(T|_y - T_\infty)}{kA_f} - \frac{(L_t)(IR)CX|_y}{kA_f}\right] \tag{56}$$

since $F(y) = IR(CX|_y)$ and the effective heat transfer coefficient from the surface is approximated as (14):

$$h_{eff} = 4\sigma\varepsilon\left(\frac{T|_y + T_\infty}{2}\right)^3 + 0.29\left(\frac{T|_y - T_\infty}{2W}\right)^{0.25} \tag{57}$$

where $T|_y$ and T_∞ are in °R

The trial and error solution results from the nonlinearity of the function and the unknown boundary condition $q_u = -kA_f dT/dy)_{y=0}$.

A more rigorous method to approximate the solution to the fin equation for a given energy distribution would be to use the implicit form of the finite differences equation and solve the resulting system of equations expressed as a tridiagonal matrix (2). This treatment is illustrated below.

The basic equation as before is Eq. (44), with F(y) replaced by (IR)[CX(y)]:

$$\frac{d^2T}{dy^2} = \frac{2h_{eff}L_t}{kA_f}(T - T_\infty) - \frac{L_t(IR)[CX(y)]}{kA_f} \tag{58}$$

Expressing the y boundary conditions in dimensionless form, Eqs. (44.1) and (44.2) become at

$$y = 0 \qquad \text{or } Y' = 0, \qquad T = t_{wall} \tag{59.1}$$

$$y = \pm y_o \text{ or } \ell \qquad \text{or } Y' = \pm 1, \qquad \frac{dT}{dy} = \frac{dT}{dY} = 0 \tag{59.2}$$

The finite difference equation can be written as:

$$\frac{T_{i-1} - 2T_i + T_{i+1}}{(\Delta Y')^2} = \frac{2y_o^2 h_{eff} L_t}{kA_f}(T_i - T_\infty) - \frac{L_t y_o^2 (IR)}{kA_f}[CX(\frac{y}{y_o})] \tag{59}$$

where $h_{eff} = f(T_i)$ and $CX = f(Y')$. Defining

$$H_1 = \frac{2L_t y_o^2}{kA_f}$$

and

$$H_2 = \frac{L_t y_o^2 (IR)}{kA_f}$$

The coefficients of the tridiagonal matrix are therefore:

$$A(1) = 1; \qquad B(1) = C(1) = 0; \qquad D(1) = t_{wall}$$

$$A(i) = C(i) = 1; \qquad B(i) = -[2 + (\Delta Y')^2 H_1 h_{eff}|_{T_i}];$$

$$D(i) = (\Delta Y')^2 [H_1 h_{eff}|_{T_i}(-T_o) - H_2 CX|_{Y'}]$$

$$A(n) = 1; \qquad B(n) = -1; \qquad C(n) = 0; \qquad D(n) = 0$$

$CX|_y$ must also be evaluated for all i (0 to n). This may be done through the use of a Lagrangian interpolating polynomial to obtain values between the discrete values of CX derived from Eq. (12) (see Appendix 10.4.4). The solution of the tridiagonal matrix gives values for T_i for the grid.

10.4.4 Computer Program Listings and Sample Output

SØL.F4

```
C     PRØGRAM TØ DETERMINE THE TEMPERATURE DISTRIBUTIØN ØN
C     A FINNED TUBE USING EULER'S METHØD TØ APPRØXIMATE THE
C     TEMPERATURE DERIVATIVES BETWEEN Y AND Y+DY
      REAL K,IR
      DIMENSIØN CX(14),T(14),DT(14),DTF(14),CXF(14),TF(14)
C     INPUT VALUES ØF CØNCENTRATIØN FACTØR,CX, FØR DISCRETE
C     VALUES ØF Y (CX VALUES ØBTAINED FRØM PRØGRAM SØLAR.F4)
      DATA CX/0.,0.,0.,0.,0.,25.8,32.,22.1,16.3,
     1 14.5,10.3,4.,2.2,0.9/
C     INPUT INITIAL GUESS FØR TEMPERATURE DISTRIBUTIØN ALØNG
C     FIN FØR DISCRETE VALUES ØF Y
      DATA T/191.,200.,211.,222.,234.,243.,249.,252.,255.,256.,
     1 257.,257.,257.,257./
C     A=AREA ØF FIN,SQ.FT
C     W=WIDTH ØF FIN,FT
C     E=EMISSIVITY ØF FIN
C     IR=INCIDENT RADIATIØN UPØN REFLECTØR,BTU/SQ.FT-HR
C     TW=TEMPERATURE ØF TUBE WALL,DEG.F
C     TØ=TEMPERATURE ØF AIR INSIDE BØX,DEG.F
C     VH=VERTICAL HEIGHT ØF BØTH FINS+TUBE,FT
C     K=THERMAL CØNDUCTIVITY ØF FIN,BTU/FT-HR-DEG.F
C     H=STEP INCREMENT ALØNG FIN,FT
C     N=NUMBER ØF STEPS ALØNG FIN
      W=7.5
      A=0.00615
      E=0.87
      IR=250.
      TØ=150.
      TW=191
      VH=0.16
      K=60.
      H=0.00417
      Y=0.0
      N=14
C     HCØ=CØNVECTIVE HEAT TRANSFER CØEFFICIENT INITIALIZED
C         AT TW,BTU/SQ.FT-HR-DEG.F
      HCØ=0.29*((TW-TØ)/VH)**0.25
C     HEFFØ=EFFECTIVE HEAT TRANSFER CØEFFICIENT INCLUDING
C           RADIATIØN,BTU/SQ.FT-HR-DEG.F
      HEFFØ=4.*0.1714E-8*E*((TW+TØ+920.)/2.)**3.+HCØ
      DT(1)=2.*HEFFØ*W*(TW-TØ)/(K*A)
      DØ 600 J=1,N
      HC=0.29*((T(J)-TØ)/VH)**0.25
      HEFF=4.*0.1714E-8*E*((T(J)+TØ+920.)/2.)**3.+HC
      Q1=2.*HEFF*W*(T(J)-TØ)/(K*A)
      Q2=W*IR*CX(J)/(K*A)
```

SØLAR.F4 (Continued)

```
02500          DT(J+1)=DT(J)+H*(Q1-Q2)
02600          Y=Y+H
02900      600 CØNTINUE
03000          Y=0.7
03100          DT(N)=0.0
03200          DØ 650 I=1,N
03300          L=N+1-I
03400          DTF(L)=DT(I)
03500          CXF(L)=CX(I)
03600          TF(L)=T(I)
03650      650 CØNTINUE
03660          DTF(1)=0.0
03670          DØ 800 L=1,N
03700          TF(L+1)=TF(L)-H*DTF(L)
03800          Y=Y-H
03900          TYPE 700,TF(L+1),Y
04000      700 FØRMAT(' TF = ',F10.5,5X,'Y = ',F10.5)
04100      800 CØNTINUE
04200          STØP
04300          END


00010    C     PRØGRAM TØ DETERMINE THE ENERGY DISTRIBUTIØN ALØNG
00020    C     A FINNED TUBE. THE CØNCENTRATIØN FACTØR,CX, IS
00030    C     GIVEN AS A FUNCTIØN ØF THE Y INTERCEPT B.
00100          TYPE 100
00200      100 FØRMAT(5X,'X',9X,'DX',8X,'PE',/)
00210    C     INPUT: X=DISTANCE ALØNG PARABØLIC SURFACE,IN
00220    C              (ØNLY 1/2 THE DISTANCE ALØNG THE SURFACE IS
00230    C               CØVERED PER RUN)
00240    C            DX=STEP INCREMENT,IN
00250    C            PE=PØINTING ERRØR,DEG.
00300          ACCEPT 200,X,DX,PE
00400      200 FØRMAT(3G)
00500          TYPE 300
00600      300 FØRMAT(//,' DISTANCE X',10X,'INTERCEPT B',
00601         19X,'CX FACTØR',/)
00700          N=X/DX
00800          X=0.0
00850          B2=0.0
00900          PE=PE/57.3
01000          DØ 500 I=1,N
01100          X=X+DX
01200          CT=CØS(PE)/SIN(PE)
01300          C=CT*(X/15.53-3.88/X)-1.0
01400          D=CT+X/15.53-3.88/X
01500          B=0.0644*X**2.-X*C/D
01550          CX=ABS(1.0/(B2-B)*DX)
01600          TYPE 400,X,B,CX
01650          B2=B
01700      400 FØRMAT(F10.5,10X,F10.5,10X,F10.5)
01800      500 CØNTINUE
01900          STØP
02000          END
```

Table 11. SØLAR.F4 Computer Output for 5° Pointing Error

X	DX	PE
9.25	0.500	5.00

DISTANCE X	INTERCEPT B	CX FACTØR
0.50000	12.07841	0.04140
1.00000	5.92312	0.08123
1.50000	5.08805	0.59875
2.00000	4.76998	1.57201
2.50000	4.61087	3.14252
3.00000	4.52195	5.62291
3.50000	4.47077	9.76888
4.00000	4.44274	17.83850
4.50000	4.43041	40.54485
5.00000	4.42962	635.16378
5.50000	4.43793	60.18689
6.00000	4.45383	31.44344
6.50000	4.47639	22.16511
7.00000	4.50502	17.46557
7.50000	4.53935	14.56108
8.00000	4.57920	12.54964
8.50000	4.62444	11.05128
9.00000	4.67506	9.87795

X	DX	PE
-9.25	-0.500	5.00

DISTANCE X	INTERCEPT B	CX FACTØR
-0.50000	2.29537	0.21783
-1.00000	2.85952	0.88629
-1.50000	3.10416	2.04384
-2.00000	3.23353	3.86468
-2.50000	3.30780	6.73241
-3.00000	3.35091	11.59964
-3.50000	3.37417	21.49613
-4.00000	3.38355	53.30890
-4.50000	3.38242	443.71257
-5.00000	3.37278	51.88257
-5.50000	3.35584	29.51381
-6.00000	3.33232	21.25956
-6.50000	3.30265	16.84867
-7.00000	3.26703	14.03904
-7.50000	3.22556	12.05528
-8.00000	3.17820	10.55821
-8.50000	3.12487	9.37566
-9.00000	3.06542	8.41065

Table 12. Temperature Distribution for Upper Fin for a 5° Pointing Error

Y (in.)	Concentration Factor, CX	T (°F)
0.00	0	190
0.05	0	199
0.10	0	208
0.15	0	217
0.20	0	226
0.25	25.8	235
0.30	32.0	242
0.35	22.1	247
0.40	16.3	250
0.45	14.5	252
0.50	10.3	252
0.55	4.0	252
0.60	2.2	252
0.65	0.9	252

Table 13. Temperature Distribution for Lower Fin for a 5° Pointing Error

Y (in.)	Concentration Factor, CX	T (°F)
0.00	0	191
0.05	0	200
0.10	0	211
0.15	0	222
0.20	24.7	234
0.25	42.7	243
0.30	24.0	249
0.35	18.8	252
0.40	13.4	255
0.45	11.0	256
0.50	11.0	257
0.55	2.7	257
0.60	2.7	257
0.65	2.7	257

10.5 Location of Original Data

The original data are located in ORNL Databook A-6977-G. The results, calculations, and the databook are on file at the M.I.T. School of Chemical Engineering Practice, Bldg. 3001, ORNL.

10.6 Dimensions and Properties of Materials

10.6.1 Flat Plate Collector

Collector Plate:

Length, L_C = 4.17 ft
Width, W_C = 1.42 ft
Effective thickness, X_C = 0.0063 ft
Area, A' = 5.90 ft^2

Box:

Length, L_B = 5.15 ft
Width, W_B = 2.15 ft
Depth, D_B = 0.70 ft
Wood Thickness, X_W = 0.0625 ft
Area (below collector plate), A'_W = 17.1 ft^2

Insulation:

Thickness, X'_I = 0.42 ft
Length, L_I = 5.02 ft
Width, W_I = 2.02 ft
Area, A'_I = 10.1 ft^2

Effective Glass Surface:

Length, L_G = 5.02 ft
Width, W_G = 1.84 ft
Thickness, X_G = 0.0104 ft
Area, A'_G = 9.23 ft^2

10.6.2 Parabolic Collector

Reflector:

Aperture, W_{REF} = 1.54 ft
Length, L_{REF} = 7.51 ft
Depth, D_{REF} = 0.46 ft
Area, A = 11.57 ft
Equation of parabola, $y = X^2/15.53$

Receiver:

Tube length, L_T	=	7.51 ft
Inside tube diameter, ID_T	=	0.0295 ft
Outside tube diameter, OD_T	=	0.0459 ft
Fin length, ℓ	=	7.51 ft
Fin width, W_F	=	0.0575 ft
Fin thickness, X_F	=	0.00082 ft
Area, A_R	=	2.76 ft^2

Box:

Length, L_B	=	8.13 ft
Width, W_B	=	2.20 ft
Depth, D_B	=	1.21 ft
Thickness, X_B	=	0.0625 ft
Glass support along length	=	0.0583 ft
Area, A_W	=	42.88 ft^2

Insulation:

Thickness, X_I	=	0.104 ft
Area, A_I	=	37.31 ft^2

Effective Glass Surface:

Length, L_G	=	8 ft
Width, W_G	=	1.96 ft
Thickness, X_G	=	0.0104 ft
Area, A_G	=	15.68 ft^2

10.6.3 Equipment Characteristics

Heat Exchanger:

Length	=	1.74 ft
Shell inside diameter	=	0.052 ft
Tube inside diameter	=	0.026 ft
Tube outside diameter	=	0.031 ft

Tank capacity = 4 gal

10.6.4 Material Properties

Thermal Conductivity:

Parabolic receiver tube	=	29.5 Btu/ft-hr-°F
Parabolic receiver fin	=	68.8 Btu/ft-hr-°F
Heat exchanger tube	=	230 Btu/ft-hr-°F
Heat exchanger shell	=	29.5 Btu/ft-hr-°F
Glass	=	0.55 Btu/ft-hr-°F

Insulation (fiberglass) = 0.023 Btu/ft-hr-°F
Box (wood) = 0.07 Btu/ft-hr-°F
f = 0.76 (for h^{o}_{air} = 1 Btu/ft^2-hr-°F)
Reflectivity of reflector (specular) = 0.87
Reflectivity of top of insulation (effective) = 0.75

Emissivity:

Parabolic Reflector = 0.09 (212°F)
Parabolic Receiver = 0.87 (392°F)
Flat plate collector = 0.98
Glass = 0.94 (72°F)

Absorptivity (at or near normal incidence):

Parabolic receiver = 0.87
Flat plate collector = 0.98

Heat Transfer Coefficients:

Outside convective, glass and box underside surface-to-air (3 mph wind speed) = 1 Btu/ft^2-hr-°F

C factor (dependent on tilt angle, β, and spacing, Btu/hr-ft^2-°F$^{5/4}$) inside convective; flat plate-to-glass (β = 20.5°, 18°) = 0.175 Btu/ft^2-hr-°F

Inside convective coefficient under collector surface to the top of insulation, h^{i}_{air} = 1 Btu/hr-ft^2-°F

Inside convective coefficient above collector surface to the glass plate surface (parabolic), h^{i}_{air} = 0.235 Btu/hr-ft^2-°F

γ, angle of reflected radiation from receiver = 197°

10.7 Nomenclature

NOTE: Primes denote flat plate collector system variables.

a angle relative to surface of parabolic reflector, deg

A, A' area of collector, ft^2

A" azimuth of the sun, deg

A'_G, A_G, A_R, A_{REF} = area of glass, receiver, reflector, ft^2

A_I, A'_I cross-sectional insulation area, ft^2

A_W, A'_W area of wood (excluding area of wood above collector plate), ft^2

A_f cross-sectional area of fin, ft^2

b	y intercept, in.
B	turbidity
c	constant dependent upon the tilt angle of the collector, directly proportional to h^i_{air}
CX	geometrical concentration factor, dimensionless
C_p	heat capacity of air, Btu/lb-°F
D_B	depth of flat plate box, ft
D_{REF}	depth of reflector, ft
Eff'	theoretical efficiency
Eff_{OBS}, Eff'_{OBS}	= efficiency of collector based on total radiation corrected for orientation
f	ratio of thermal resistance of outer glass plate to that of the inner plate
$F(y)$	energy distribution function, Btu/ft^2
h	altitude of the sun, deg
h^i_{air}	natural inside convection coefficient, Btu/hr-ft^2-°F
$h^i_{air,B}$	box natural inside convection coefficient, Btu/hr-ft^2-°F
h^o_{air}	forced and natural outside convection coefficient, Btu/hr-ft^2-°F
h_c	convective heat transfer coefficient, Btu/hr-ft^2-°F
h_{eff}	effective heat transfer coefficient including radiation, Btu/hr-ft^2-°F
H	step increment along fin, in.
H_{D_1}	direct radiation incident on pyrheliometer, Btu/hr-ft^2
H_D	direct radiation corrected for orientation, Btu/hr-ft^2
H_{DIF}	diffuse radiation obtained from pyrheliometer, Btu/hr-ft^2
H_{DIF_1}	diffuse radiation from clouds, Btu/hr-ft^2
H_{DIF_2}	diffuse radiation when clear (no clouds), Btu/hr-ft^2
H_T	total radiation incident on collector plate or reflector corrected for orientation, Btu/hr-ft^2

H_{TOT} total radiation incident on pyrheliometer, Btu/hr-ft^2

IR incident radiation hitting reflector, Btu/hr-ft^2

k thermal conductivity of fin, Btu/hr-ft-°F

k_G, k_I, k_w = thermal conductivity of glass, insulation, and wood, Btu/hr-ft-°F

$\ell = y_o$ width of fin, ft

L_B, L_C, L_G, L_I, L_{REF}, L_t = length of box, flat plate collector, glass, insulation, reflector, and finned tube, ft

$\dot{m}$ mass flow rate of water corrected for viscosity change, lb/hr

n total number of glass plates

n' number of glass plates for parabolic collector

p coordinate of focal point of parabolic mirror, in.

q_A, q_A',(Q_A, Q_A') = total energy absorbed by collector surface, Btu/hr, (Btu)

q_B, q_B',(Q_B, Q_B') = heat loss from the collector surface through the insulation below it and out the bottom of the box, Btu/hr, (Btu)

q_G, q_G' heat loss from the collector surface through the glass plates to the atmosphere, Btu/hr

q_u, q_u' useful heat in the working fluid of the collector system, Btu/hr

$(q_u)_{EXPT}$, (Q_u) = observed heat gained by working fluid, Btu/hr, (Btu)

r specular reflectivity of reflector

r_{eff} effective reflectivity of aluminum foil

R distance coordinate, in.

RA right ascension of the sun, deg

R_D orientation factor for direct radiation

R_S orientation factor for diffuse radiation

t time, hr

t_{wall} temperature of finned tube wall, °F

T temperature, °F or °R

T_o ambient temperature, °F

T_2 surface temperature under glass plate 1, °F

T_3, T_3' temperature of glass plate 2, °F

T_4, T_4' temperature of air space above collector, °F

T_5, T_5' average collector temperature, °F

T_6 average receiver temperature, °F

T_7, T_6' temperature at top of insulation, °F

T_8, T_7' underside of insulation temperature, °F

T_9, T_8' underside of box temperature, °F

T_1' temperature of glass plate 1, °F

T_{in}, T_{in}' inlet working fluid temperature, °F

T_{LM} log mean theoretical temperature of flat plate collector, °F

T_{out}, T_{out}' outlet working fluid temperature, °F

V average penetration through a cloud ($\sim$0.5)

w width of fin, ft

W_C, W_B, W_G, W_I, W_{REF} = width of collector plate, box, glass, insulation, and reflector, ft

X_G, X_I, X_I', X_w = thickness of glass, insulation, wood, ft

y distance coordinate, in. or ft

y_o width of fin, ft

Y sky cover (range 1 to 10)

Y' dimensionless distance coordinate

$\alpha(\alpha_S')$ overall absorptivity of black collector receiver for direct (diffuse) radiation

β tilt angle of collector, deg

γ angle determining portion of radiation emitted by receiver which is intercepted by the reflector, deg

δ declination angle of the sun, deg

$\varepsilon_C, \varepsilon_G, \varepsilon_R$	emissivity of collector plate, glass, and receiver
θ_T	angle of solar incidence on tilted surface, deg
θ_Z	angle of solar incidence on horizontal surface, deg
Λ	shape factor; the ratio of reflected radiation intercepted by the receiver to the radiation specularly reflected by the reflector
§	pointing angle
σ	Stefan-Boltzmann constant, 0.1714×10^{-8} Btu/hr-ft^2-°R^4
$\tau_e(\tau_{e_s})$	overall effective transmittance for direct (diffuse) radiation
Φ	latitude (36°03' for Oak Ridge), deg
Ψ	pointing angle error, deg
ω	local hour angle of the sun, deg
Γ	vernal equinox

10.8 Temperature Measurements

Table 14 gives the average temperature measurements for the parabolic focusing collector and the flat plate collector.

10.9 References

1. Blanco, V.M., and S.W. McCuskey, "Basic Concepts of the Solar System," Addison-Wesley, New York (1961).

2. Carnahan, B., H.A. Luther, and J.O. Wilkes, "Applied Numerical Methods," Wiley, New York (1969).

3. Culkowski, W.M., personal communication, AEC, May 1974.

4. Culkowski, W.M., computer output of total radiation incident on a pyrheliometer.

5. "Daily, Monthly, and Annual Climatological Data for Oak Ridge, Tenn., Townsite, and Area Stations January 1951 through December 1971," U.S. Dept. of Commerce, National Oceanic and Atmospheric Administration (July 1972).

6. "F&P Tri-Flat Flowmeter Handbook," Catalog 10A9010, Fischer and Porter, Hatboro, Penn.

TABLE 14. AVERAGE TEMPERATURE MEASUREMENTS

Time Interval	Temperature Readings of Parabolic Focusing Collector (°F)[a]													Temperature Readings of Flat Plate Collector (°F)[a]							
	$(T_{out})_{av}$	$(T_{in})_{av}$	$(\Delta T)_{av}$	$(T_1)_{av}$ {T_8}	$(T_2)_{av}$	$(T_3)_{av}$ {T_5}	$(T_4)_{av}$	$(T_5)_{av}$	$(T_6)_{av}$ {T_6}	$(T_7)_{av}$	$(T_8)_{av}$ {T_2}	$(T_9)_{av}$ {T_9}	$(T_{10})_{av}$ {T_o}	(T'_2) {$(T'_{out})_{av}$}	(T'_1) {$(T'_{in})_{av}$}	- {$(\Delta T')_{av}$}	(T'_4) {T'_5}	(T'_3) {T'_6}	(T'_5) {T'_7}	(T'_{12}) wood {T'_8}	(T_o) ambient {T'_o}
5-7-74 11:36-11:49	182	83	99	79	131	126	99	249	345	177	117	67	67	186	80	106	182	181	69	62	67
5-8-74 12:23-12:39	162	93	69	93	154	153	136	237	317	182	155	77	77	157	92	65	139	134	90	72	77
5-13-74 12:00-12:16	166	109	57	86	135	133	123	235	289	184	108	73	75	167	108	59	153	147	76	69	75
14:28-14:55	184	117	67	94	146	148	155	253	183	201	119	77	80	185	117	68	190	186	86	76	80
15:05-15:41	165	121	44	94	143	150	157	232	163	222	119	78	83	166	122	44	179	173	88	77	83
16:34-16:59	132	102	30	95	126	135	133	179	132	204	107	75	87	134	106	28	130	123	85	74	87
5-14-74 10:23-10:55	138	84	54	81	124	116	92	226	183	146	98	70	72	135	84	51	125	118	72	69	72
11:35-12:09	166	96	70	90	141	138	122	262	358	189	111	76	79	167	96	71	150	143	89	75	79
13:10-13:30	185	108	77	96	147	148	140	267	292	220	118	79	82	185	108	77	175	169	87	79	82
15:20-15:42	164	121	43	97	143	151	158	242	160	227	119	81	88	163	123	40	154	147	91	83	88

[a]Values in ( ) are thermocouple numbers. Values in { } are used in heat loss equations.

7. Fraas, A.P., G. Samuels, and J.V. Wilson, "Conceptual Design for a Solar Total Energy System," ORNL-HUD (1973).

8. Hilsmeier, W.F., "Supplementary Meteorological Data for Oak Ridge," USAEC-ORO-199 (1963).

9. Hottel, H.C., and B.B. Woertz, "The Performance of Flat-Plate Solar-Heat Collectors," Trans. ASME, 64, 91 (1942).

10. Hottel, H.C., and A. Whillier, "Evaluation of Flat-Plate Solar-Collection Performance," Solar-Energy-Conversion Research Project, Publication 53, Mass. Institute of Technology, Cambridge (1953).

11. Duffie, J.A., G.O.G. Löf, and E.M.A. Salam, "Solar Heat Exchangers," Chem. Eng. Progr., 56, 63 (1960).

12. Löf, G.O.G., D.A. Fester, and J.A. Duffie, "Energy Balances on a Parabolic Cylinder Solar Collector," Trans. ASME, 84, 24 (Jan. 1962).

13. Kaplan, K.J., H. Ozog., and U. Bühlmann, "Design and Utilization of a Cylindrical Parabolic Focusing Solar Energy Collection System," ORNL-MIT-186 (March 1974).

14. McAdams, W.H., "Heat Transmission," 3rd ed., McGraw-Hill, New York (1954).

INTERNAL DISTRIBUTION

1. S.I. Auerbach
2. S.E. Beall
3. H.W. Bertini
4. W.M. Culkowski, AEC
5. F.L. Culler
6. D.M. Eissenberg
7-11. A.P. Fraas
12. F.A. Gifford, Jr., AEC
13. J.S. Johnson, Jr.
14. R.S. Livingston
15. A.J. Miller
16. F.L. Miller
17. R.E. Minturn
18. E.D. Mott
19. D.J. Nelson
20. E. Newman
21. C.B. Pollock
22. H. Postma
23. M.W. Rosenthal
24. T.H. Row
25. G. Samuels
26. J.L. Sharp, AEC
27. D.B. Trauger
28. G.J. Werner
29. J.V. Wilson
30-31. Central Research Library
32. Document Reference Section
33-35. Laboratory Records
36. Laboratory Records, ORNL R.C.
37. ORNL Patent Office
38-57. M.I.T. Practice School

EXTERNAL DISTRIBUTION

58. E. Lumsdaine, U.T.
59. R.L. Reid, U.T.
60. J.E. Vivian, MIT